Intramolecular Charge Transfer with 4-Fluorofluorazene and the Flexible 4-Fluoro-*N*-phenylpyrrole

Sergey I. Druzhinin,*,†,‡ Sergey A. Kovalenko,*,§ Tamara A. Senyushkina,† Attila Demeter,‖ Regis Januskevicius,⊥ Peter Mayer,# Dietmar Stalke,▽ Reinhard Machinek,○ and Klaas A. Zachariasse*,†

Spektroskopie und Photochemische Kinetik, Max-Planck-Institut für biophysikalische Chemie, 37070 Göttingen, Germany, Institut für Chemie, Humboldt Universität zu Berlin, Brook-Taylor Strasse 2, 12489 Berlin, Germany, Institute of Materials and Environmental Chemistry, Chemical Research Center, Hungarian Academy of Sciences. P.O. Box 17, 1525 Budapest, Hungary, Department of Nonlinear Optics and Spectroscopy, Institute of Physics, Savanoriu Avenue 231, LT-02300 Vilnius, Lithuania, Department Chemie und Biochemie, Ludwig-Maximilians-Universität, Butenandtstrasse 5-13, Haus F, 81377 München, Germany, Institut für Anorganische Chemie, Universität Göttingen, Tammannstrasse 4, and Institut für Organische Chemie, Universität Göttingen, Tammannstrasse 2, 37077 Göttingen, Germany

Received: April 20, 2009; Revised Manuscript Received: May 28, 2009

With 4-fluorofluorazene (FPP4F) and its flexible counterpart 4-fluoro-*N*-phenylpyrrole (PP4F) an intramolecular charge transfer (ICT) reaction occurs in the singlet excited state in sufficiently polar solvents. The ICT reaction begins to appear in tetrahydrofuran ($\varepsilon = 7.4$) for FPP4F and in the more polar 1,2-dichloroethane ($\varepsilon = 10.4$) with PP4F, showing its presence by dual fluorescence from a locally excited (LE) and an ICT state. Only LE fluorescence is observed in less polar solvents such as *n*-hexane. The ICT reaction is more pronounced with FPP4F than for PP4F, due to the smaller energy gap $\Delta E(S_1,S_2)$ of the former molecule, in accordance with the PICT model. The occurrence of an ICT reaction is confirmed by the ICT dipole moments μ_e(ICT) of 12 D (FPP4F) and 10 D (PP4F), clearly larger than μ_e(LE) of ∼4 D for FPP4F and PP4F. Isoemissive points are found in the fluorescence spectra of FPP4F and PP4F in acetonitrile (MeCN), ethyl cyanide (EtCN), and *n*-propyl cyanide (PrCN) as a function of temperature, confirming the two-state (LE and ICT) reaction mechanism. From plots of the logarithm of the ICT/LE fluorescence quantum yield ratio versus the reciprocal absolute temperature in these solvents, the ICT reaction enthalpies ΔH are determined, with larger $-\Delta H$ values for FPP4F than for PP4F: 19.2 as compared with 14.9 kJ/mol in MeCN, as an example. The picosecond fluorescence decay of PP4F at −45 °C becomes slower with decreasing solvent polarity, 5.1 ps (MeCN), 14 ps (EtCN), and 35 ps (PrCN), from which the LE → ICT reaction rate constant is calculated, decreasing from 19×10^{10} to 2.1×10^{10} s^{-1} between MeCN and PrCN. The femtosecond LE excited-state absorption spectra of FPP4F and PP4F do not undergo any time development in *n*-hexane (no ICT reaction), but show a fast ICT reaction in MeCN at 22 °C, with decay times of 1.1 ps (FPP4F) and 3.3 ps (PP4F). It is concluded that FPP4F and PP4F have a planar ICT state (PICT model), indicating that a perpendicular twist of the donor and acceptor subgroups in a donor/acceptor molecule is not a requirement for fast and efficient ICT. The molecular structures of FPP4F and PP4F obtained from X-ray crystal analysis reveal that the pyrrole group of PP4F is twisted over an angle $\theta = 25°$ relative to the fluorophenyl moiety in the ground state, whereas as expected FPP4F is practically planar ($\theta = 2°$). The pyrrole−phenyl bond length of FPP4F (140.7 pm) is shorter than that for PP4F (141.8 pm).

Introduction

By introducing a $-CH_2-$ bridge linking the phenyl and pyrrole moieties of *N*-phenylpyrrole (PP), the planarized and rigidized molecule fluorazene (FPP) is produced (Chart 1). With the electron donor (D)/acceptor (A) molecule FPP, efficient intramolecular charge transfer (ICT) is observed in sufficiently polar solvents such as acetonitrile (MeCN) and ethyl cyanide (EtCN).[1] The ICT reaction rate constant k_a of FPP is in fact considerably larger than that of its flexible counterpart PP. In EtCN at −45 °C, for example, the locally excited (LE) → ICT reaction rate constant $k_a = 8.2 \times 10^{10}$ s^{-1} for FPP (reaction time $1/k_a = 12$ ps) and 3.7×10^{10} s^{-1} for PP (reaction time equal to 27 ps).[1] This shows that the rigidization introduced into FPP leads to faster ICT than that observed with PP in this

CHART 1

* To whom correspondence should be addressed. E-mail: sdruzhi@gwdg.de (S.I.D.); skovale@chemie.hu-berlin.de (S.A.K.); kzachar@gwdg.de (K.A.Z.). Fax: +49-551-201-1501.
† Max-Planck-Institut für biophysikalische Chemie.
‡ Affiliation: Chemistry Department, Moscow State University, 119991 Moscow, Russia.
§ Humboldt Universität zu Berlin.
‖ Hungarian Academy of Sciences.
⊥ Institute of Physics.
Ludwig-Maximilians-Universität.
▽ Institut für Anorganische Chemie, Universität Göttingen.
○ Institut für Organische Chemie, Universität Göttingen.

10.1021/jp903613c CCC: $40.75
Published on Web 07/30/2009

solvent, indicating that a perpendicular twist of the phenyl and pyrrole subgroups is not a requirement for fast and efficient ICT with these molecules.

In the case of the pair 4-cyanofluorazene (FPP4C) and 4-cyano-*N*-phenylpyrrole (PP4C), fast ICT already takes place in the nonpolar solvent *n*-hexane, with a reaction time of 0.65 ps (FPP4C) and 0.48 ps (PP4C) as determined from excited-state absorption (ESA) measurements.[2] For FPP and PP, in contrast, an ICT reaction does not occur in this solvent.[1,3,4] In the polar MeCN, the ICT reaction of FPP4C and PP4C has become ultrafast, at the limit of the experimental time resolution (around 50 fs) of the transient absorption measurements. The decay times obtained from the band integrals in the ESA spectra of FPP4C and PP4C, with a short time around 80 fs and a longer time between 360 and 900 fs, are similar to the dielectric relaxation times of 89 and 630 fs of the solvent MeCN and hence do not directly reflect the intrinsic ICT reaction time but are limited by dielectric relaxation.[2] These molecules therefore cannot be investigated by picosecond fluorescence decay measurements, having a time resolution of around 3 ps.[5] This has the disadvantage that experiments as a function of temperature, giving information on the reaction thermodynamics such as the ICT activation energy E_a and the ICT reaction enthalpy ΔH, cannot be carried out with FPP4C and PP4C.[2]

The increase in ICT efficiency for the pair FPP4C/PP4C as compared with FPP/PP is caused by the larger electron acceptor strength of benzonitrile relative to benzene, as deduced from their reduction potentials $E(A^-/A)$ of -2.36 and -3.42 V vs SCE, respectively.[6−12] A similar influence of the introduction of a cyano group is encountered when going from *N*,*N*-dimethylaniline (DMA) to 4-(dimethylamino)benzonitrile (DMABN). Whereas DMA does not undergo an ICT reaction,[13,14] efficient ICT is found with DMABN[5,15] in sufficiently polar solvents.[15−19]

To obtain a fluorazene/*N*-phenylpyrrole pair with a somewhat slower and hence experimentally more accessible ICT reaction than for FPP4C and PP4C, 4-fluorofluorazene (FPP4F) was synthesized and compared with 4-fluoro-*N*-phenylpyrrole (PP4F). It was expected, in view of the fact that a F atom is a substantially weaker electron acceptor substituent than a cyano group,[20] that the ICT reaction of FPP4F and PP4F would be slower than that for FPP4C and PP4C and would therefore be suitable for our picosecond fluorescence and femtosecond transient absorption measurements. Relative to FPP and PP,[1] on the other hand, a more efficient ICT reaction is expected for FPP4F/PP4F.

In the present paper, the results of photostationary and time-resolved fluorescence and ESA measurements with FPP4F, PP4F, and 4-methyl-*N*-phenylpyrrole (PP4M) are reported. These ESA spectra also serve to verify the identification of the previously published ESA bands of FPP4C and PP4C in *n*-hexane, the identification of which proved to be difficult, because of spectral overlap and ultrafast kinetic equilibration of the LE and ICT states.[2] PP4M does not undergo an ICT reaction in any solvent and is hence employed as a model compound for the LE ESA band. The photophysical meaning of "LE state" has been treated in ref 12.

Experimental Section

7-Fluoro-9*H*-pyrrolo[1,2-*a*]indole (4-fluorofluorazene, FPP4F) was synthesized as follows. 2-Amino-5-fluorobenzoic acid (Aldrich) was reacted with 2,5-dimethoxytetrahydrofuran (Aldrich) in acetic acid, giving 5-fluoro-2-(1*H*-pyrrol-1-yl)benzoic acid.[22] This product was treated with PCl_5 in toluene. After addition of $SnCl_4$,[23] 7-fluoro-9*H*-pyrrolo[1,2-*a*]indol-9-one was obtained, which was added to a solution of semicarbazide hydrochloride (Aldrich) in ethanol and refluxed for 6 h to give the semicarbazone. This compound together with KOH was heated to 210 °C in diethylene glycol, resulting under evolution of nitrogen in FPP4F, mp 68.8−69.2 °C. In the following NMR data, chemical shifts are in parts per million and couplings in hertz. See Chart 2 for the atom numbering. ^{1}H NMR (600 MHz, $CDCl_3$): (FPP4F) 3.82 (s (br), 2H12, $J_{12,F} = 0.91$), 6.093 (m, H10, $J_{10,9} = 3.30$, $J_{10,8} = 1.08$, $J_{10,12} = 1.50$), 6.356 (dd, H9, $J_{9,10} = 3.30$, $J_{9,8} = 2.80$), 6.98 (ddt, H5, $J_{5,6} = 8.50$, $J_{5,3} = 2.50$, $J_{5,12} = 0.70$, $J_{5,F} = 9.05$), 7.035 (m, H8, $J_{8,9} = 2.80$, $J_{8,10} = 1.08$, $J_{8,12} = 0.94$), 7.105 (m, H3, $J_{3,5} = 2.50$, $J_{3,12} = 1.10$, $J_{3,F} = 8.25$), 7.153 (dd, H6, $J_{6,5} = 8.50$, $J_{6,F} = 4.4$); (PP4F) 6.408 (m, BB′, H8, H11), 7.06 (m, AA′, H9, H10), 7.15 (m, AA′, H2, H6, $J_{2,3} = 9.0$, $J_{2,6} = 2.57$, $J_{2,F} = 4.6$, $J_{3,F} = 8.15$), 7.37 (m, BB′, H3, H5, $J_{3,5} = 3.32$). ^{13}C NMR (500 MHz, $CDCl_3$, ^{1}H broad-band decoupled): (FPP4F) 29.3 (C12, $^4J_{12,F} = 2.08$), 102.0 (C10), 109.9 (C6, $^3J_{6,F} = 8.75$), 113.1 (C9), 113.6 (C3, $^2J_{3,F} = 24.51$), 113.7 (C5, $^2J_{5,F} = 23.99$), 135.4 (C11), 136.8 (C2, $^3J_{2,F} = 8.66$), 137.5 (C1, $^4J_{1,F} = 1.51$), 159.4 (C4, $^1J_{4,F} = 240.7$), 169.7 (C8); (PP4F) 110.42 (C9, C10), 116.17 (C3, C5, $^2J_{3,F} = 22.68$), 119.51 (C8, C11), 122.14 (C2, C6, $^3J_{2,F} = 8.34$), 137.08 (C1, $^4J_{1,F} = 2.74$), 160.54 (C4, $^1J_{4,F} = 244.60$). ^{19}F NMR (282 MHz, $CDCl_3$): (FPP4F) −120.5 (dddt, F13); (PP4F) −117.00 (tt, F13). The HH and HF couplings were determined by analysis and simulation of the spectra.

The purification of FPP4F, PP4F (Alfa Aesar), and PP4M (Aldrich) was carried out as described before,[24] with HPLC as the last purification step. All solvents were chromatographed over Al_2O_3 just prior to use. The solutions, having an optical

CHART 2

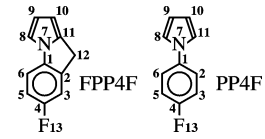

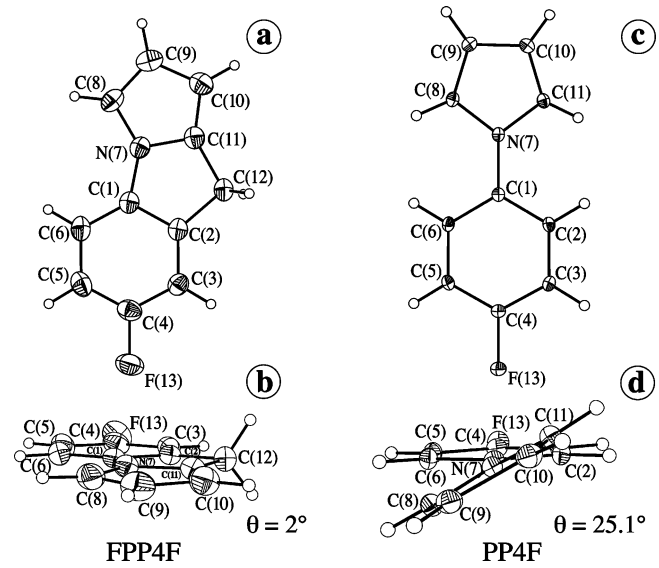

Figure 1. Crystal structures of FPP4F and PP4F. For these molecules, a view from above (a, c) and one along the axis from the pyrrole nitrogen to the fluoro substituent (b, d) are presented. The amino twist angle θ is defined as (C(2)−C(1)−N(7)−C(11) + C(6)−C(1)−N(7)−C(8))/2. The pyramidal angle φ is the angle between the vector N(7)−C(1) and the plane through C(8)−N(7)−C(11); see Table 1.

TABLE 1: Experimental Data for the Ground-State Structures of FPP4F and PP4F from X-ray Crystal Analysis[a]

	FPP4F	PP4F[b]	PP4F[c]	PP4F[d]	FPP4C[e]	PP4C[f]	PP4C[g]	PP[h]
N(7)−C(1)	140.7	141.8	141.6	142.0	139.9	140.7	140.6	142.3
N(7)−C(8)	137.0	138.0	137.8	138.1	138.5	137.9	138.2	137.9
N(7)−C(11)	138.4	138.0	137.8	138.1	138.2	137.9	138.2	137.9
C(1)−C(2)	139.2	139.4	139.6	139.3	139.8	139.4	139.0	139.4
C(1)−C(6)	137.8	139.4	139.6	139.3	138.4	139.4	139.0	139.4
C(2)−C(3)	138.1	139.0	139.0	139.1	138.1	138.5	138.8	138.9
C(3)−C(4)	137.8	137.8	138.1	137.5	140.6	139.6	138.9	138.8
C(4)−C(5)	137.2	137.8	138.1	137.5	140.0	139.6	138.9	138.8
C(5)−C(6)	139.1	139.0	139.0	139.1	139.3	138.5	138.8	138.9
C(8)−C(9)	136.3	137.1	137.1	137.0	136.7	137.0	135.5	136.2
C(9)−C(10)	142.0	141.9	141.9	141.9	142.3	140.8	141.1	141.2
C(10)−C(11)	136.2	137.1	137.1	137.0	135.9	137.0	135.5	136.2
C(11)−C(12)	149.9				150.8			
C(2)−C(12)	151.7				152.2			
C(4)−F(13)	136.2	135.9	135.8	135.9				
C(4)−C(13)					144.1	143.2	144.6	
C(13)−N(14)					115.0	114.7	111.6	
C(1)−N(7)−C(8)	138.5	125.8	125.8	125.8	137.9	125.7	126.2	126.3
C(1)−N(7)−C(11)	111.3	125.8	125.8	125.8	112.0	125.7	126.2	125.8
C(8)−N(7)−C(11)	110.1	108.4	108.4	108.4	110.1	108.6	107.5	107.9
$\sum N^i$	359.9	360.0	360.0	360.0	360.0	360.0	360.0	360.0
twist angle θ^j	2.0	25.1	27.9	22.3	1.0	24.2	24.0	5.7
pyramidal angle φ^k	3.0	0.0	0.0	0.0	0.2	0.0	0.0	0.3
quinoidality[l]	1.014	1.009	1.006	1.011	0.995	0.992	0.999	1.001

[a] Data for FPP4C, PP4C, and PP are also presented. See the atom numbering in Chart 2 and Figure 1. The bond lengths are in picometers, and the angles are in degrees. [b] Mean value for the two independent molecules in the asymmetric unit of PP4F.[27] [c] For molecule A of the two independent molecules in the asymmetric unit. [d] For molecule B of the two independent molecules in the asymmetric unit. [e] From ref 2. [f] From ref 28. [g] From ref 29. [h] From ref 4. [i] Sum of the angles around the pyrrole nitrogen (Figure 1). [j] Twist angle θ = (C(6)−C(1)−N(7)−C(8) + C(6)−C(1)−N(7)−C(11))/2 (Figure 1). [k] The pyramidal angle φ is the angle between the vector N(7)−C(1) and the plane C(8)−N(7)−C(11) (Figure 1). [l] Quinoidality = (C(5)−C(6))/(C(4)−C(5)) (Figure 1).

density between 0.4 and 0.6 at the maximum of the first band in the absorption spectrum, were deaerated by bubbling with nitrogen for 15 min. The measurement and treatment of the fluorescence spectra and quantum yields, intersystem crossing yields Φ(ISC), single-photon-counting (SPC) decays, and femtosecond transient absorption spectra has been described elsewhere.[4−6,25,26] The transient absorption spectra were measured at room temperature (∼22 °C).

Results and Discussion

Molecular Structure of FPP4F and PP4F. The molecular structure of FPP4F and PP4F, determined by X-ray crystal analysis, is depicted in Figure 1. The pyrrole subgroup of PP4F is twisted relative to the phenyl moiety over an angle θ of 25.1° ((27.91 + 22.31)/2). As to be expected, FPP4F is practically planar, with a twist angle θ of 2.0° (Table 1). A similar planarization has been observed for FPP4C (1.0°) as compared with PP4C (24.2°).[2,28,29]

Pyrrole−Phenyl Bond Length. The pyrrole−phenyl bond length C(1)−N(7) in the series PP (142.3 pm), PP4F (141.8 pm), and PP4C (140.7 pm) decreases with increasing acceptor strength of the substituent at C(4). The same trend is observed for FPP4F (140.7 pm) and FPP4C (139.9 pm). Somewhat surprisingly, the twist angle θ is larger for PP4F (25.1°) and PP4C (24.2°) than for PP (5.7°), notwithstanding the larger double bond character of the C(1)−(N7) bond for the two former molecules.

Absorption Spectra of PP4F and FPP4F at 25 °C. $\Delta E(S_1,S_2)$. The absorption spectrum of PP4F in *n*-hexane consists of a main band with a maximum $\tilde{\nu}^{max}$(abs) at 40870 cm^{-1} (ε^{max} = 12800 M^{-1} cm^{-1}) and a weaker transition as a shoulder at the low-energy side of the spectrum (Figure 2a and Table 2). A similar spectrum is found in diethyl ether (DEE), tetrahydrofuran (THF), and MeCN (Figure 2b−d). For FPP4F in *n*-hexane (Figure 2e), the spectrum likewise consists of a strong band with maxima at 38510 and 39490 cm^{-1} (ε^{max} = 13930 and 13770 M^{-1} cm^{-1}) and a weaker structured absorption at lower energies, with maxima at 32660 and 33940 cm^{-1} (ε^{max} = 2660 and 2790 M^{-1} cm^{-1}). These spectra are similar to those of the pairs PP/FPP and PP4C/FPP4C.[1−3]

Following the identification of the two absorption bands of PP,[2,4] the main band of FPP4F and PP4F is attributed to the $S_0 \rightarrow S_2$ transition, whereas the red-edge shoulder is due to the $S_0 \rightarrow S_1$ absorption. From *n*-hexane to MeCN, the S_1 band of FPP4F gradually loses its structure (Figure 2e−h). The maximum shifts to higher energies with increasing solvent polarity: 33940 cm^{-1} (*n*-hexane), 33980 cm^{-1} (DEE), 34030 cm^{-1} (THF), and 34290 cm^{-1} (MeCN).

The energy difference $\tilde{\nu}^{max}(S_2,abs) - E(S_1)$ between the maximum of the S_2 absorption and the energy $E(S_1)$, see Table 2, is taken as an approximation for the energy gap $\Delta E(S_1,S_2)$ between the two lowest excited singlet states.[2] In *n*-hexane, $\Delta E(S_1,S_2)$ is smaller for FPP4F (5940 cm^{-1}) than with PP4F (6690 cm^{-1}). A similar observation has been made for FPP4C (1260 cm^{-1}) as compared with PP4C (1710 cm^{-1}).[2] From the decrease in $\Delta E(S_1,S_2)$ of FPP4F relative to PP4F a more efficient ICT reaction is to be expected for the former molecule.[1−6,9]

Amino Twist Angle of PP4F from Comparison with Planarized FPP4F. Absorption Coefficients. The twist angle θ between the pyrrole and benzonitrile groups of PP4F in the S_0 ground state in solution can be determined from the absorption coefficient ε^{max} relative to that (ε^{max}(ref)) of the planarized FPP4F as its reference compound with approximately zero twist angle (Table 2). This approach, based on eq 1, has previously been used to estimate θ for FPP4C[2] and the nonplanar 4-(2,5-dimethylpyrrolyl)benzonitrile,[30] 1-*tert*-butyl-6-cyano-1,2,3,4-tetrahydroquinoline (NTC6),[24] the 4-aminobenzonitriles 3,5-

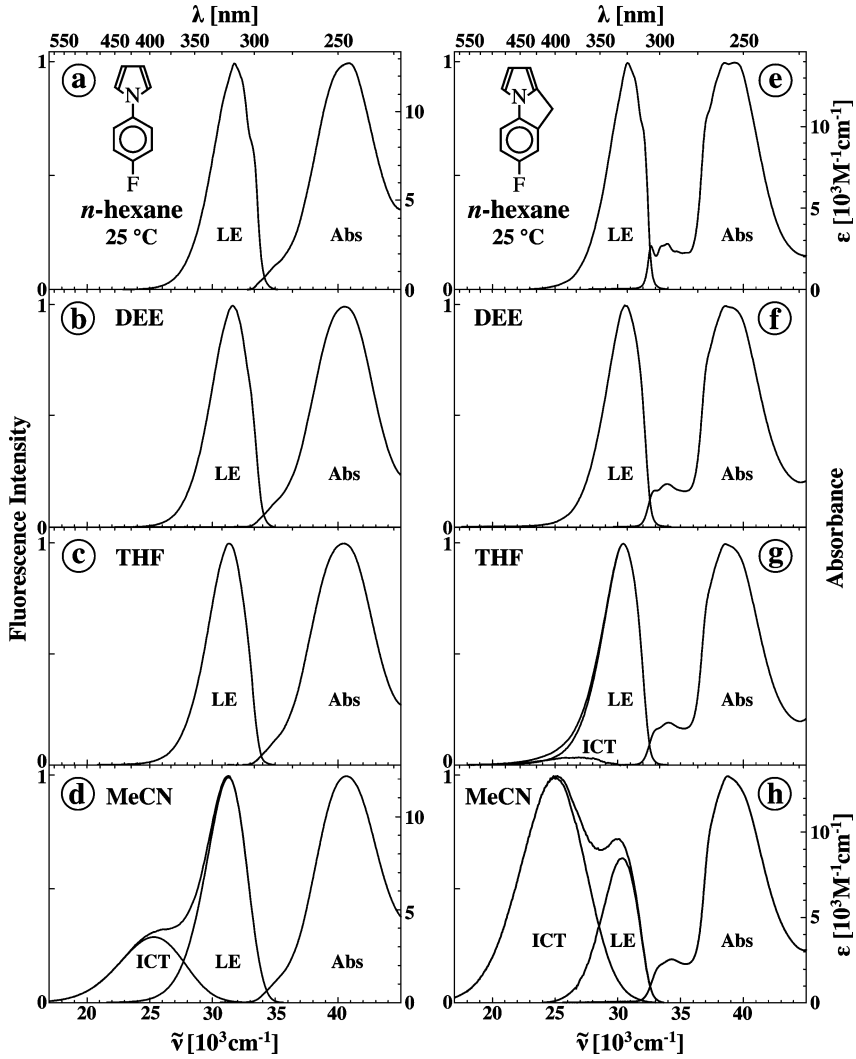

Figure 2. Absorption (Abs) and fluorescence spectra of PP4F (a−d) and FPP4F (e−h) in *n*-hexane (a, e), DEE (b, f), THF (c, g), and MeCN (d, h) at 25 °C. The overall fluorescence spectra of PP4F in (d) and FPP4F in (g) and (h) are separated into the contributions from the LE and ICT states. This separation is carried out by employing the spectrally shifted LE band of PP4M as a model for the LE emission of PP4F and with the spectrally shifted LE emission band of FPP (d) as the LE model for FPP4F. The excitation wavelength λ(exc) is around 270 nm.

dimethyl-4-(methylamino)benzonitrile (MHD) and 3,5-dimethyl-4-(dimethylamino)benzonitrile (MMD),[31] and 1-(dimethylamino)-naphthalene and its derivatives[32] in solution.

$$\varepsilon^{max}/\varepsilon^{max}(\text{ref}) = \cos^2\theta \qquad (1)$$

From the data for ε^{max} of FPP4F (13850 M^{-1} cm^{-1}, mean value) and PP4F (12800 M^{-1} cm^{-1}) in *n*-hexane at 25 °C (Table 2), a twist angle θ of 16° is calculated for PP4F (eq 1). The ε^{max} values in MeCN (13260 vs 12220 M^{-1} cm^{-1}, Table 2) lead to practically the same result of 16.5°. These findings for θ in solution compare favorably with the twist angle of 25.1° obtained from X-ray crystallography (Table 1) and may indicate that PP4F is in fact somewhat more planar in solution than in the crystal. A similar conclusion is made for PP and PP4C. Whereas amino twist angles $\theta = 5.7°$ (PP) and $\theta = 24°$ (PP4C) were determined in the crystal, a planar configuration ($\theta = 0°$) was deduced from the extinction coefficients ε^{max} of both molecules in solution.[2,4]

Fluorescence Spectra of PP4F and FPP4F at 25 °C. As mentioned in the Introduction, PP and FPP do not undergo ICT in *n*-hexane, dual fluorescence from an LE and an ICT state only starting to appear clearly in solvents more polar than THF ($\varepsilon^{25} = 7.39$).[1,4] In the case of PP, the ICT/LE fluorescence quantum yield ratio Φ'(ICT)/Φ(LE) at 25 °C equals 0.10 in 1,2-dichloroethane (DClE; $\varepsilon^{25} = 10.4$).[33] A similar situation is encountered here with PP4F and FPP4F (Figure 2). The limiting solvent, where dual fluorescence just becomes visible for PP4F at 25 °C, is DClE, with Φ'(ICT)/Φ(LE) = 0.03 (Table 3), whereas ICT emission starts to appear for FPP4F in the somewhat less polar THF, with Φ'(ICT)/Φ(LE) = 0.05 (Figure 2g, Table 3). For PP4F in this solvent, the presence of an additional ICT fluorescence band on the red edge of the LE emission cannot be detected with certainty (Figure 2c).[34] These results show that the ICT efficiency is enhanced by the presence of the methylene linker in FPP4F, the same observation as previously made for the pairs FPP/PP and FPP4C/PP4C.[1,2] This can also be seen by comparing Φ'(ICT)/Φ(LE) in MeCN at 25 °C, which for FPP4F is 2.5 much larger than that of PP4F of 0.46 (Tables 2 and 3). Similar results were obtained for FPP4F relative to PP4F in *n*-butyl cyanide (BuCN), *n*-propyl cyanide (PrCN), EtCN, *N*,*N*-dimethylformamide (DMF), ethanol, and methanol (Table 3).

Solvatochromic Measurements. LE and ICT Dipole Moments of FPP4F and PP4F. For the determination of the dipole moments μ_e(ICT) and μ_e(LE) of FPP4F and PP4F, the maximum $\tilde{\nu}^{max}$(ICT) or $\tilde{\nu}^{max}$(LE) of the fluorescence bands was determined in a series of solvents, from the nonpolar *n*-hexane ($\varepsilon^{25} = 1.88$)

TABLE 2: Data Obtained from the Fluorescence and Absorption Spectra of FPP4F and PP4F in a Series of Solvents[a]

	FPP4F							PP4F						
	n-hexane	DEE	THF	PrCN	EtCN	MeCN	MeCN[b]	*n*-hexane	DEE	THF	PrCN	EtCN	MeCN	MeCN[b]
$\tilde{\nu}^{max}$(LE) (cm^{-1})	30770	30660	30410	30430	30390	30360	30530	31800	31650	31310	31110	31080	31230	31250
$\tilde{\nu}^{max}$(ICT) (cm^{-1})			(26550)	25790	25400	24920	24410				25110	25210	25280	24740
Φ(LE)	0.21	0.19	0.15	0.048	0.027	0.013	0.0013	0.13	0.15	0.15	0.081	0.068	0.026	0.0046
Φ′(ICT)	0	0	0.008	0.020	0.025	0.032	0.038	0	0	0	0.003	0.007	0.012	0.014
Φ′(ICT)/Φ(LE)	0	0	0.05	0.42	0.91	2.5	30	0	0	0	0.04	0.10	0.46	3.0
Φ(ISC)[c]	0.79	0.80				0.96		0.86	0.83				0.95	
$-\Delta H$(SB)[d] (kJ/mol)				16.5	13.6	19.2					12.6	14.0	14.9	
$\tilde{\nu}^{max}$(S_1,abs) (cm^{-1}) (nm)	32660 (306.2)	32950 (303.5)	32980 (303.2)	34150	34190	34290	34330							
	33940 (294.6)	33980 (294.3)	34030 (293.9)	(292.8)	(292.4)	(291.7)	(291.3)							
ε^{max}(S_1,abs) (M^{-1} cm^{-1})	2660	0.164[e]	0.156[e]	0.188[e]	0.187[e]	2520	2630							
	2790	0.195[e]	0.192[e]											
$\tilde{\nu}^{max}$(S_2,abs) (cm^{-1}) (nm)	38510 (259.7)													
	30490 (253.2)	38640 (258.8)	38570 (259.3)	38660 (258.6)	38680 (258.5)	38750 (258.1)	38750 (258.1)	40870 (244.7)	40480 (247.0)	40400 (247.5)	40460 (247.2)	40530 (246.7)	40640 (246.1)	40550 (246.6)
	⟨39000⟩													
ε^{max}(S_2,abs) (M^{-1} cm^{-1})	13930					13260	13700	12800					12150	13140
	13770													
$E(S_1)$[f] (cm^{-1})	32570	32600	32510	32660	32680	32590		34180	34130	33880	33810	33880	34080	33940
$\Delta E(S_1,S_2)$[g] (cm^{-1})	5940	6040	6060	6000	6000	6160		6690	6290	6520	6650	6650	6560	6610
E(FC,ICT)[h] (kJ/mol)				66	74	79					87	85	93	

[a] Solvents: diethyl ether (DEE), tetrahydrofuran (THF), *n*-propyl cyanide (PrCN), ethyl cyanide (EtCN), acetonitrile (MeCN). Data are at 25 °C, unless otherwise indicated. [b] At −45 °C. [c] Measurements as in ref 4. Φ(ISC) for PP4M: 0.54 (*n*-hexane), 0.41 (DEE), 0.60 (MeCN), ref 4. Data uncertainty ±0.05. [d] Enthalpy difference between LE and ICT, determined from a plot of ln(Φ′(ICT)/Φ(LE)) vs 1000/T (eq 5a). [e] Relative to the absorbance at $\tilde{\nu}^{max}$(S_2,abs). [f] Crossing point of the normalized fluorescence and absorption spectra (Figure 2). [g] The energy difference $\tilde{\nu}^{max}$(abs) − $E(S_1)$ is taken as an approximation for the energy gap $\Delta E(S_1,S_2)$ between the two lowest excited singlet states (refs 2 and 12). [h] Energy of the Franck−Condon (FC) state reached upon ICT emission. E(FC,ICT) = $E(S_1)$ + (ΔH) − $\tilde{\nu}^{max}$(ICT); see eq 6 and Figure 8.

TABLE 3: ICT and LE Fluorescence Maxima $\tilde{\nu}^{max}$(ICT) and $\tilde{\nu}^{max}$(LE) of FPP4F, PP4F, and DIABN at 25 °C in a Series of Solvents Spanning the Polarity Scales $f(\varepsilon) - {}^1/_2 f(n^2)$ for ICT and $f(\varepsilon) - f(n^2)$ for LE (Eqs 2−4)

					FPP4F			PP4F			DIABN[a]
solvent	ε	n	$f(\varepsilon) - {}^1/_2 f(n^2)$	$f(\varepsilon) - f(n^2)$	$\tilde{\nu}^{max}$(ICT) (1000 cm^{-1})	$\tilde{\nu}^{max}$(LE) (1000 cm^{-1})	Φ′ (ICT)/Φ(LE)[b]	$\tilde{\nu}^{max}$(ICT) (1000 cm^{-1})	$\tilde{\nu}^{max}$(LE) (1000 cm^{-1})	Φ′ (ICT)/Φ(LE)[b]	$\tilde{\nu}^{max}$(ICT) (1000 cm^{-1})
n-hexane (1)	1.88	1.372	0.092	0.000		30.77	0		31.77	0	25.72
cyclopentane (2)	1.96	1.404	0.097	−0.001		30.89	0		31.52	0	25.57
diethyl ether (3)	4.24	1.350	0.253	0.165		30.66	0		31.65	0	23.52
n-butyl acetate (4)	4.95	1.392	0.266	0.170		30.65	0		31.51	0	22.61
tetrahydrofuran (5)	7.39	1.405	0.307	0.208	(26.6)	30.40	0.05		31.49	0	22.38
1,2-dichloroethane (6)	10.4	1.443	0.326	0.221	26.21	30.39	0.23	(25.70)	31.31	(0.03)	21.65
n-butyl cyanide (7)	19.8	1.395	0.366	0.270	25.88	30.44	0.33	25.70	31.31	0.04	21.30
n-propyl cyanide (8)	24.2	1.382	0.375	0.281	25.79	30.43	0.53	25.58	31.11	0.06	21.09
ethyl cyanide (9)	29.2	1.363	0.384	0.293	25.40	30.39	0.83	25.50	31.11	0.13	20.87
acetonitrile (10)	36.7	1.342	0.393	0.306	24.92	30.31	2.5	25.28	31.23	0.46	20.49
dimethylformamide (11)	36.7	1.428	0.377	0.275	25.13	30.17	1.70	25.29	31.14	0.48	20.49
ethanol (12)	24.6	1.360	0.380	0.289	25.04	29.63	0.15	25.13	31.47	0.04	20.31
methanol (13)	32.7	1.326	0.393	0.309	24.59	29.16	0.91	24.97	31.43	0.14	19.86

[a] From ref 6. [b] ICT/LE fluorescence quantum yield ratio (eq 5a).

to the strongly polar MeCN and dimethylformamide (ε^{25} = 36.7); see Table 3.

$$\tilde{\nu}^{max}(\text{flu}) = -\frac{1}{2hc\rho^3}\mu_e(\mu_e - \mu_g)g(\varepsilon, n) + \text{const} \quad (2)$$

$$f(\varepsilon) = \frac{\varepsilon - 1}{2\varepsilon + 1} \quad (3)$$

$$f(n^2) = \frac{n^2 - 1}{2n^2 + 1} \quad (4)$$

In eq 2, μ_g and μ_e are the ground- and excited-state dipole moments, ε is the dielectric constant, n is the refractive index, ρ is the Onsager radius of the solute, and $g(\varepsilon,n) = f(\varepsilon) - {}^1/_2 f(n^2)$ for μ_e(ICT) and $f(\varepsilon) - f(n^2)$ for μ_e(LE).[3,6,39,41]

From the slope of the plot of $\tilde{\nu}^{max}$(ICT) of FPP4F vs the solvent polarity parameter $f(\varepsilon) - {}^1/_2 f(n^2)$ (eqs 2−4),[3,35−38] μ_e(ICT) = 12.0 D is determined (Figure 3a). By plotting $\tilde{\nu}^{max}$(ICT) against that of 4-(diisopropylamino)benzonitrile (DIABN) (μ_e(ICT) = 18 D)[39] in this series (Figure 3b), the same μ_e(ICT) = 12.1 D is calculated; see Table 4. With this last procedure, the scatter in the data points is generally reduced by mutually compensating the specific solute/solvent interactions.[6,35,39,40] For PP4F, a somewhat smaller ICT dipole moment of 11.0 D vs $f(\varepsilon) - {}^1/_2 f(n^2)$ and of 9.2 D relative to DIABN is obtained.

The LE dipole moment μ_e(LE) of FPP4F is determined in a manner similar to the procedure followed for μ_e(LE): 4.3 D from $\tilde{\nu}^{max}$(LE) vs $f(\varepsilon) - f(n^2)$ and 4.6 D vs $\tilde{\nu}^{max}$(ICT,DIABN); see

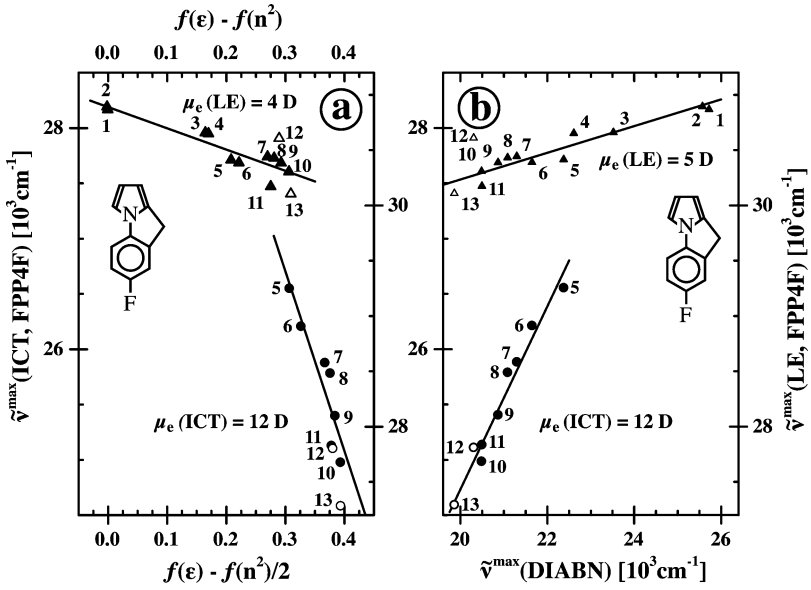

Figure 3. Solvatochromic plots of the LE fluorescence maxima $\tilde{\nu}^{max}$(LE) and the ICT fluorescence maxima $\tilde{\nu}^{max}$(ICT) of FPP4F vs (a) the solvent polarity parameter $f(\varepsilon) - f(n^2)$ for LE and $f(\varepsilon) - {}^1/_2 f(n^2)$ for ICT and (b) $\tilde{\nu}^{max}$(ICT) of DIABN (see eqs 2−4). For $\tilde{\nu}^{max}$(flu) and the numbering of the solvents, see Table 3. From the slopes of the plots, the LE dipole moment μ_e(LE) of FPP4F is calculated: 4.3 D for (a) and 4.6 D for (b). Similarly, the ICT dipole moment μ_e(ICT) of FPP4F is determined: 12 D for (a) and (b). See eq 2, Table 4, and the text. The data for the alcohol solvents 12 and 13 are not used in the calculation of the dipole moments.

TABLE 4: Data from the Solvatochromic Analysis of the ICT and LE Fluorescence Maxima of FPP4F and PP4F

	ρ^a (Å)	$\mu_g{}^b$ (D)	slope(ICT)^c	μ_e(ICT)^d (D)	slope(LE)^c	μ_e(LE)^e (D)
FPP4F (eq 2)	4.45	0.32^f	−16000 ± 3200	12.0 ± 1.0	−1900 ± 270	4.3 ± 0.3
FPP4F	4.45	0.32^f	0.83 ± 0.08	12.1 ± 0.6	0.12 ± 0.01	4.6 ± 0.2
(vs DIABN)^g	(4.68)	(6.8)		(18)		
PP4F (eq 2)	4.34	0.32^h	−14000 ± 6800	11.0 ± 2.6	−1750 ± 360	3.9 ± 0.4
PP4F	4.34	0.32^h	0.50 ± 0.02	9.2 ± 0.2	0.11 ± 0.02	4.3 ± 0.4
(vs DIABN)^g	(4.68)	(6.8)		(18)		

^{a} Onsager radius (eq 2), calculated from an effective density equal to 0.78, based on DMABN. See ref 3. ^{b} Ground-state dipole moment. ^{c} Slope for the lines through the data points in Figures 3 and 4. ^{d} ICT dipole moment (eq 2). ^{e} LE dipole moment (eq 2). ^{f} Dipole moment of PP4F; see footnote^h. ^{g} For DIABN, ρ = 4.68 Å, μ_g = 6.8 D, and μ_e(ICT) = 18 D, from refs 3 and 6. ^{h} Determined by measuring the dielectric constant ε and the refractive index n of solutions of PP4F in *p*-dioxane as a function of the solute concentration (ref 41). Dipole moments of PP4M: μ_g = 1.81 D, μ_e(LE) = 1.9 D (ref 3).

Figure 3 and Table 4 (eqs 2−4). For PP4F, μ_e(LE) = 4 D (Figure 4 and Table 4).

The occurrence of an ICT reaction with FPP4F and PP4F is confirmed by the dipole moments of their two fluorescence bands, with μ_e(ICT) = 12 D for FPP4F and μ_e(ICT) ≅ 10 D for PP4F, both considerably larger than μ_e(LE) of around 4 D for FPP4F and PP4F. A comparison with literature data shows that the μ_e(ICT) values of FPP (13 D)[1] and PP (12 D)[3] are similar to those of FPP4F/PP4F. For FPP4C (15 D)[2] and PP4C (16 D),[2] larger μ_e(ICT) values are measured, due to the stronger electron affinity of the *para*-substituent (see the Introduction).

Fluorescence Spectra of FPP4F and PP4F as a Function of Temperature. The fluorescence spectra of FPP4F and PP4F in the alkyl cyanides MeCN, EtCN, and PrCN as a function of temperature are shown in Figures 5 and 6. These spectra consist of an ICT and an LE emission band; see Figure 2h,d for the separated spectra in MeCN. The ICT emission maximum $\tilde{\nu}^{max}$(ICT) undergoes a shift to lower energies upon cooling. For FPP4F in MeCN, as an example, $\tilde{\nu}^{max}$(ICT) decreases from 25380 cm^{-1} at 80 °C to 24410 cm^{-1} at −45 °C, whereas with PP4F in this solvent $\tilde{\nu}^{max}$(ICT) goes from 25200 to 24340 cm^{-1} between these temperatures. This red shift is caused by the increase in the solvent polarity ε from 29.8 at 80 °C to 50.2 at −45 °C.[4,33,42,43]

With FPP4F in MeCN and EtCN (Figure 5a,b), the intensity of the LE fluorescence band decreases from +80 to −45 °C for MeCN and from +95 to −85 °C in EtCN, whereas the corresponding ICT emission band continuously increases upon lowering the temperature. With FPP4F in PrCN (Figure 5c), in contrast, the LE fluorescence intensity gradually decreases between +105 and −100 °C and then increases toward −112 °C. The intensity of the ICT band becomes continuously larger upon cooling from +105 to −106 °C. For the LE and ICT fluorescence of PP4F in MeCN, EtCN, and PrCN (Figure 6) a similar temperature dependence is found.

In each of the three solvents, Φ′(ICT)/Φ(LE) is substantially larger for FPP4F than for PP4F (Figures 5 and 6). At 25 °C, the following values are obtained in MeCN, EtCN, and PrCN: 2.5, 0.83, and 0.53 with FPP4F against 0.46, 0.13, and 0.06 for PP4F (Table 2). At all temperatures, Φ′(ICT)/Φ(LE) decreases when going from MeCN to PrCN, as expected[4] because of the decreasing polarity in this solvent series[42,43] (Table 3). The detailed temperature dependence of the ICT/LE fluorescence quantum yield ratio Φ′(ICT)/Φ(LE) is treated below.

Isoemissive Points. With FPP4F as well as PP4F in MeCN, EtCN, and PrCN, isoemissive points appear in the sets of fluorescence spectra presented as a function of temperature (Figures 5 and 6). This indicates that there are at least[26] two

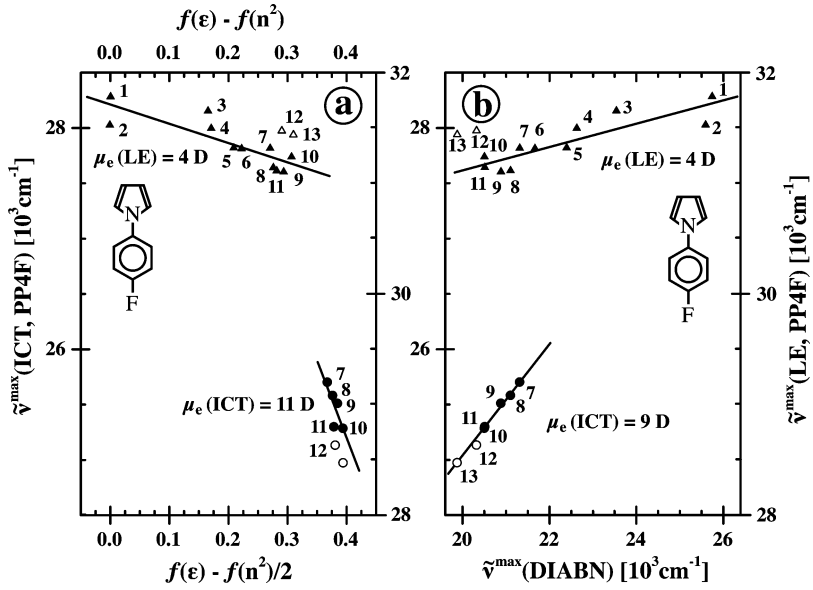

Figure 4. Solvatochromic plots of the LE fluorescence maxima $\tilde{\nu}^{max}$(LE) and the ICT fluorescence maxima $\tilde{\nu}^{max}$(ICT) of PP4F vs (a) the solvent polarity parameter $f(\varepsilon) - f(n^2)$ for LE and $f(\varepsilon) - {}^1/_2 f(n^2)$ for ICT and (b) $\tilde{\nu}^{max}$(ICT) of DIABN (see eqs 2−4). For $\tilde{\nu}^{max}$(flu) and the numbering of the solvents, see Table 3. From the slopes of the plots, the LE dipole moment μ_e(LE) of PP4F is calculated: 3.9 D for (a) and 4.3 D for (b). Similarly, the ICT dipole moment μ_e(ICT) of PP4F is determined: 11.0 D for (a) and 9.2 D for (b). See eq 2, Table 4, and the text. See the caption of Figure 3.

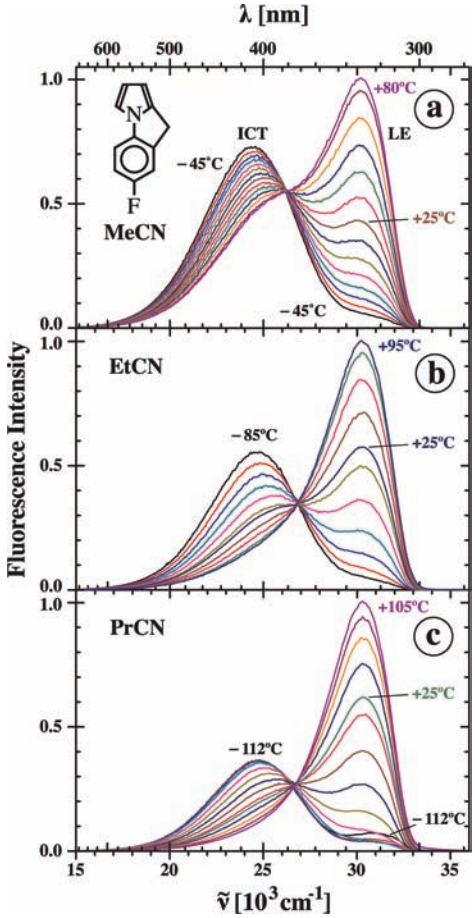

Figure 5. Fluorescence spectra as a function of temperature of FPP4F in (a) MeCN, (b) EtCN, and (c) PrCN. The spectra consist of a dual emission from an LE and an ICT state. Note the isoemissive points (see the text).

excited species involved in the ICT reaction of these molecules, in accordance with Scheme 1 comprising an LE and an ICT state.

SCHEME 1

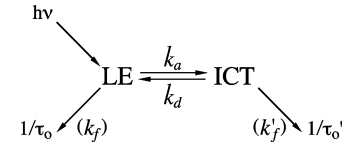

Temperature Dependence of Φ′(ICT)/Φ(LE) for FPP4F and PP4F. The quantum yield ratio Φ′(ICT)/Φ(LE) (eq 5a) of FPP4F in MeCN strongly increases upon cooling, from 0.85 at 80 °C, via 2.8 at 25 °C, to 30 at −45 °C (Figures 5a and 7a, Table 2). With PP4F in MeCN, Φ′(ICT)/Φ(LE) likewise becomes larger when the temperature is lowered, from 0.19 at 80 °C, via 0.46 at 25 °C, to 3.0 at −45 °C (Figures 6a and 7b, Table 2). A comparable temperature dependence is obtained for Φ′(ICT)/Φ(LE) with FPP4F and PP4F in EtCN: from 0.37 at 95 °C to 13.4 at −85 °C for FPP4F and from 0.08 at 34 °C to 2.07 at −89 °C for PP4F (Figures 5b, 6b, and 7).

With FPP4F in PrCN, Φ′(ICT)/Φ(LE) increases from 0.25 at 105 °C, via 0.53 at 25 °C, to 15.0 at −100 °C and then decreases again: 12.1 at −106 °C and 8.82 at −112 °C (Figures 5c and 7a). Similarly, for PP4F in PrCN Φ′(ICT)/Φ(LE) increases from 0.04 at 25 °C to 0.79 at −98 °C and then decreases to 0.66 at −109 °C (Figures 6c and 7b). With PP4F as compared to FPP4F, Φ′(ICT)/Φ(LE) is smaller at each temperature in each of the three solvents (Figures 5−7).

ICT Kinetics. HTL Condition with Small Δ*H*. The observation that Φ′(ICT)/Φ(LE) of FPP4F and PP4F in MeCN, EtCN, and PrCN increases when the temperature is lowered (Figures 5−7) indicates that these molecules are in the high-temperature limit (HTL), which holds when $k_d \gg 1/\tau_0'$(ICT) (Scheme 1).[4,10,44] This condition is an indication that the enthalpy difference Δ*H* between the LE and ICT states is relatively small. Examples of such an HTL situation are PP in MeCN (Δ*H* = −8.8 kJ/mol), EtCN (−5.9 kJ/mol), PrCN (−5.1 kJ/mol), and BuCN (−3.9 kJ/mol),[4] as well as FPP in MeCN (−15.1 kJ/mol),[1] NTC6 in *n*-hexane (−2.4 kJ/mol),[24] and DMABN in toluene[10,44] (−11.6 kJ/mol) and DEE[32b] (−17 kJ/mol). With DMABN in MeCN (Δ*H* = −27.0 kJ/mol), however, the HTL

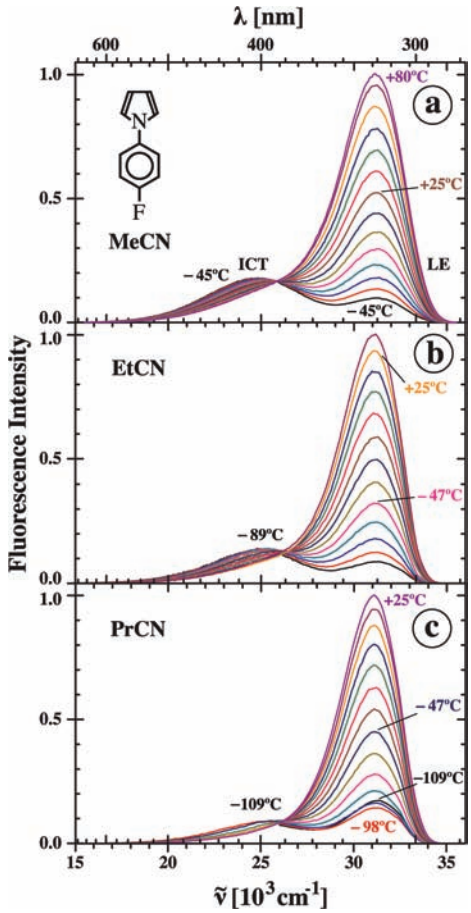

Figure 6. Fluorescence spectra as a function of temperature of PP4F in (a) MeCN, (b) EtCN, and (c) PrCN. The spectra consist of a dual emission from an LE and an ICT state. Note the isoemissive points (see the text).

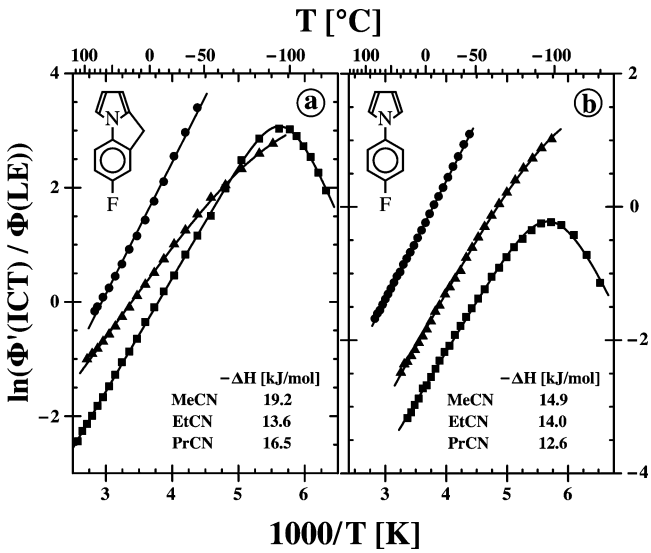

Figure 7. ln(Φ′(ICT)/Φ(LE)) vs the reciprocal absolute temperature 1000/T for (a) FPP4F and (b) PP4F in MeCN (●), EtCN (▲), and PrCN (■). The LE → ICT reaction enthalpies ΔH(SB) obtained by fitting the data with eq 5a are indicated in the figure.

does not hold at 25 °C, as k_d (0.47×10^9 s^{-1}) is only slightly larger than $1/\tau_0'$(ICT) (0.26×10^9 s^{-1}) at this temperature.[5]

In Scheme 1 and the following equation, k_a and k_d are the rate constants of the forward and backward ICT reactions, τ_0(LE) and τ_0'(ICT) are the fluorescence lifetimes, and k_f(LE) and k_f'(ICT) are the radiative rate constants:

$$\Phi'(\mathrm{ICT})/\Phi(\mathrm{LE}) = k_f'(\mathrm{ICT})/k_f(\mathrm{LE})\{k_a/(k_d + 1/\tau_0'(\mathrm{ICT}))\} \quad (5a)$$

When $k_d \gg 1/\tau_0'$(ICT), the HTL,[4,10,24,44] eq 5a simplifies to

$$\Phi'(\mathrm{ICT})/\Phi(\mathrm{LE}) = k_f'(\mathrm{ICT})/k_f(\mathrm{LE})(k_a/k_d) \quad (5b)$$

Stevens−Ban Plots for FPP4F and PP4F. ICT Reaction Enthalpy ΔH(SB). The so-called Stevens−Ban (SB)[45,46] plots of ln(Φ′(ICT)/Φ(LE)) vs 1000/[T (K)] for FPP4F in MeCN, EtCN, and PrCN are presented in Figure 7a, those of PP4F in Figure 7b. From a fitting of the plots, the enthalpy difference ΔH(SB) for the LE → ICT reaction is determined (eq 5a, Table 2). In MeCN a larger $-\Delta H$(SB) is obtained for FPP4F (19.2 kJ/mol) than with PP4F (14.9 kJ/mol), explaining the increase in the Φ′(ICT)/Φ(LE) ratio for the former system (Figure 7 and Table 3). A similar situation is found with FPP4F (16.5 kJ/mol) and PP4F (12.6 kJ/mol) in PrCN. In EtCN, somewhat surprisingly, practically the same ΔH is calculated for the two compounds, although Φ′(ICT)/Φ(LE) is througout larger for FPP4F than for PP4F (Figure 7). In PrCN, Φ′(ICT)/Φ(LE) passes through a maximum at −95 °C with FPP4F and at −97 °C for PP4F. At these temperatures, $k_d = 1/\tau_0'$(ICT). This condition is not reached for FPP4F and PP4F in MeCN and EtCN; see Figure 12 of PP4F in EtCN, for which k_d would become equal to $1/\tau_0'$(ICT) at the inacessible temperature of −104 °C, below the melting point of the solvent (−91.9 °C).

***E*(FC,ICT).** The energy E(FC,ICT), relative to the equilibrated S_0 state, of the Franck−Condon ground state populated by the ICT fluorescence (Figure 8) can be determined via the following equation, employing the data for $E(S_1) = E$(LE), ΔH, and $\tilde{\nu}^{max}$(ICT) from Table 2:

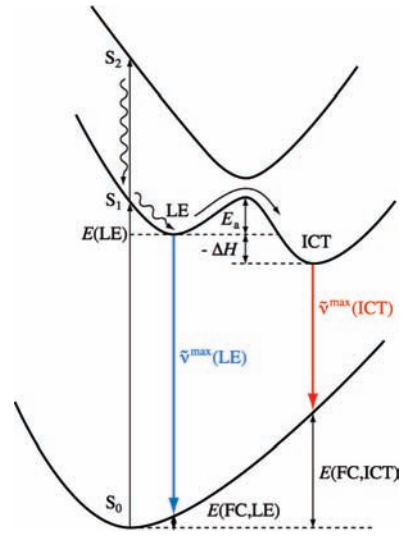

Figure 8. Potential energy surfaces for the ground state S_0 and the excited states S_1, S_2, LE, and ICT. When excited to the S_2 state (with an energy gap $\Delta E(S_1,S_2)$ above the energy of S_1), the system relaxes by internal conversion to the equilibrated LE state, having an energy E(LE) above that of S_0. The ICT reaction proceeds from the LE to the ICT state, with a reaction barrier E_a and an enthalpy difference ΔH. Fluorescence from the LE and ICT states, with emission maxima $\tilde{\nu}^{max}$(LE) and $\tilde{\nu}^{max}$(ICT), reaches the corresponding Franck−Condon states E(FC,LE) and E(FC,ICT).

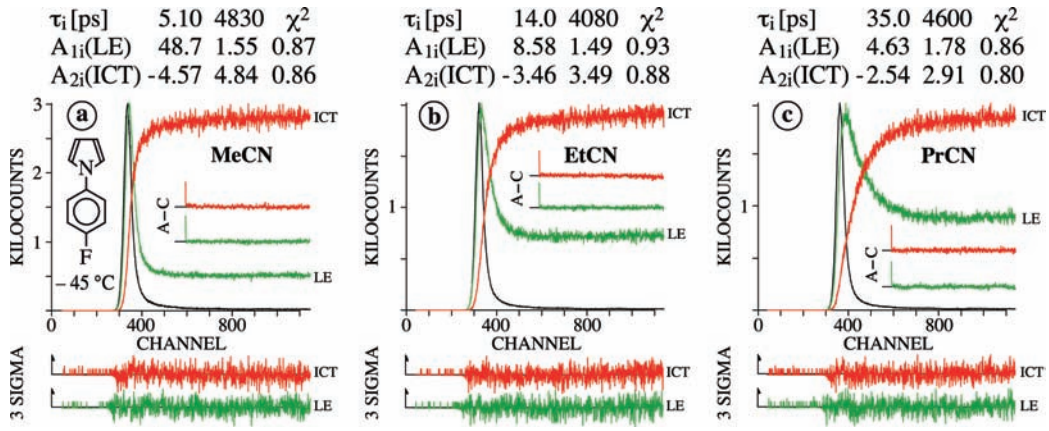

Figure 9. Global analysis for double-exponential LE and ICT fluorescence decays of PP4F at −45 °C in (a) MeCN, (b) EtCN, and (c) PrCN. The emission wavelengths are 320 nm (LE), 460 nm (ICT, MeCN, EtCN), and 450 nm (ICT, PrCN). The decay times τ_2 and τ_1 with the corresponding amplitudes A_{1i}(LE) and A_{2i}(ICT), see eqs 7−9, are given in the figure. The shortest decay time is listed first. The weighted deviations σ, the autocorrelation functions A−C, and the values for χ^2 are also indicated. The excitation wavelength is 276 nm. The time resolution is 0.496 ps/channel with a time window of 800 effective channels.

$$E(\mathrm{FC,ICT}) = E(\mathrm{S_1}) + \Delta H - \tilde{\nu}^{\max}(\mathrm{ICT}) \qquad (6)$$

For FPP4F the results are 79 kJ/mol (MeCN), 74 kJ/mol (EtCN), and 66 kJ/mol (PrCN). With PP4F somewhat higher energies are obtained: 93 kJ/mol (MeCN), 85 kJ/mol (EtCN), and 87 kJ/mol (PrCN). The large magnitude of E(FC,ICT) means that these FC states are not thermally accessible from S_0, ruling out a competitive direct ICT excitation bypassing LE; see Figure 8.[11,47,48] The lower E(FC,ICT) values found for FPP4F as compared with PP4F can indicate that the structural changes involved in the LE → ICT reaction are smaller for the rigidized molecule.

Picosecond LE and ICT Fluorescence Decays of PP4F in Alkyl Cyanides at −45 °C. The global analysis of the LE and ICT picosecond fluorescence decays i_f(LE) and i_f(ICT) of PP4F in MeCN, EtCN, and PrCN at −45 °C is shown in Figure 9. From the decay times τ_2 and τ_1, their LE amplitude ratio $A = A_{12}/A_{11}$, and the fluorescence lifetime τ_0 of PP4F in isooctane (no ICT reaction), the ICT rate constants k_a and k_d, as well as the ICT lifetime τ_0'(ICT) can be calculated (Scheme 1, eqs 7−16). The results for k_a, k_d, and τ_0'(ICT) are collected in Table 5.

$$i_f(\mathrm{LE}) = A_{11}\exp(-t/\tau_1) + A_{12}\exp(-t/\tau_2) \qquad (7)$$

$$i_f(\mathrm{LE}) = A_{21}\exp(-t/\tau_1) + A_{22}\exp(-t/\tau_2) \quad \text{with} \quad A_{22} = -A_{21} \qquad (8)$$

$$A = A_{12}/A_{11} \qquad (9)$$

The expressions for τ_1, τ_2, and A appearing in eqs 7−9 are[5,44,46]

$$1/\tau_{1,2} = \frac{1}{2}\{(X + Y) \mp \sqrt{(X - Y)^2 + 4k_a k_d}\} \qquad (10)$$

$$A = \frac{X - 1/\tau_1}{1/\tau_2 - X} \qquad (11)$$

$$X = k_a + 1/\tau_0 \qquad (12)$$

$$Y = k_d + 1/\tau_0'(\mathrm{ICT}) \qquad (13)$$

$$k_a = (1/\tau_1 + A/\tau_2)/(1 + A) - 1/\tau_0 \qquad (14)$$

$$k_d = \{(1/\tau_1 + 1/\tau_1)^2 - (2k_a + 2/\tau_0 - 1/\tau_1 - 1/\tau_0)^2\}/4k_a \qquad (15)$$

$$1/\tau_0'(\mathrm{ICT}) = 1/\tau_1 + 1/\tau_2 - k_a - k_d - 1/\tau_0 \qquad (16)$$

where τ_0 is the fluorescence lifetime of the model compound (no ICT) and X and Y are given by the following two equations.

The short decay time τ_2 increases for PP4F in the alkyl cyanide solvent series (Figure 9): 5.1 ps (MeCN), 14.0 ps (EtCN), and 35 ps (PrCN). At the same time, the amplitude ratio A (eq 11) decreases: 31.4 (MeCN), 5.8 (EtCN), and 2.6 (PrCN). This means that the rate constant k_a for the LE → ICT reaction becomes smaller (Table 5), caused by a lowering of the solvent polarity ε(−45 °C): 50.2 (MeCN), 39.0 (EtCN), and 35.1 (PrCN).[42]

LE/ICT Fluorescence Decay Analysis for PP4F in Alkyl Cyanides at −45 °C. The LE and ICT fluorescence decays of PP4F in MeCN, EtCN, and PrCN at −45 °C are double-exponential (Figure 9). As a further proof that only the two states LE and ICT are involved in the excited-state reaction (Scheme 1), the ICT decay i_f(ICT) has been deconvoluted with the LE decay i_f(LE) as a formal excitation pulse profile.[4,49,50] A single-exponential LE/ICT decay is obtained in the three solvents (Figure 10), with a decay time τ(LC); see eq 17 and Table 5. A good agreement between the experimental τ(LC) and the calculated $1/(k_d + 1/\tau_0'(\mathrm{ICT}))$ is found (Table 5, eq 17). These results show that for an analysis of the ICT reaction with

TABLE 5: Fluorescence Decay Parameters τ_2, τ_1, A, and τ_0, Eqs 7−13, Scheme 1, ICT Reaction Rate Constants k_a and k_d, ICT Lifetime τ_0'(ICT), LE/ICT Decay Time τ(LC) (Eq 17), Free Enthalpy Difference ΔG, and Enthalpy Difference ΔH for FPP4F, PP4F, FPP, PP, and DMABN in Isooctane, PrCN, EtCN, and MeCN

	T (°C)	τ_2 (ps)	τ_1 (ns)	A	τ_0(PP4F)[a] (ns)	τ_0(PP4M) (ns)	k_a (10^{10} s^{-1})	k_d (10^{10} s^{-1})	τ_0'(ICT)(ns)	τ(LC)[b] (ps)	ΔG[c] (kJ/mol)	ΔH[d] (kJ/mol)
						FPP4F						
isooctane	25		5.13		5.13							
EtCN	−45	2.8	6.79	40.6	5.64		34.8	0.86	6.81	150 (115)	−7.0	−13.6 (SB)
EtCN	−85	6.4	7.99	108	5.96		15.5	0.14	8.02	707 (642)	−7.4	
MeCN	−45	2.02	7.42	75.8	5.64		48.8	0.64	7.45	(152)	−8.2	−19.2 (SB)
						PP4F						
isooctane	25		5.15		5.15							
PrCN	−45	35.0	4.60	2.60	5.75		2.1	0.79	4.27	124 (124)	−1.8	−12.6 (SB)
EtCN	−45	14.0	4.08	5.76	5.75		6.1	1.05	3.88	96 (93)	−3.3	−14.0 (SB)
EtCN	−85	29.8	4.72	25.9	5.96		3.2	0.12	4.68	715 (690)	−5.2	−14.0
MeCN	−45	5.10	4.83	31.4	5.75		19.0	0.60	4.81	155 (160)	−6.6	−14.9 (SB)
						FPP						
EtCN[e]	−45	11	13.08	9.03		11.73	8.2	0.9	13.4	108 (110)	−4.2	
MeCN												−15.1 (SB)
						PP[f]						
PrCN	−45	31.3	7.38	0.71		11.77	1.33	1.85	4.86	56 (53)	+0.63	−4.6
EtCN	−45	15.4	6.41	1.42		11.73	3.88	2.66	4.87	35 (37)	−0.72	−6.7
MeCN	−45	8.7	5.88	6.39		11.66	9.92	1.55	5.46	67 (64)	−3.5	−10.0
						DMABN[g]						
MeCN	−45	7.63	3.53	14472[i]		3.72[h]	13.08	0.0009	3.53	(3421)[j]	−18.2	−27.0

[a] Decay times measured in isooctane (no ICT reaction). [b] The value in parentheses is the calculated decay time $\tau(\mathrm{LC}) = 1/(k_d + 1/\tau'_0(\mathrm{ICT}))$ (eq 17). [c] $\Delta G = -RT \ln(k_a/k_d)$. [d] Values with "(SB)" come from plots of $\Phi'(\mathrm{ICT})/\Phi(\mathrm{LE})$ vs $1000/T$ (eq 5a, Table 2). [e] From ref 1. [f] From refs 4 and 33. [g] From ref 5. [h] Decay time of 4-(methylamino)benzonitrile (ref 5). [i] Estimated from data in ref 5. [j] Experimental τ(LC) not accessible because of too high LE amplitude ratio A (eq 9); see ref 5.

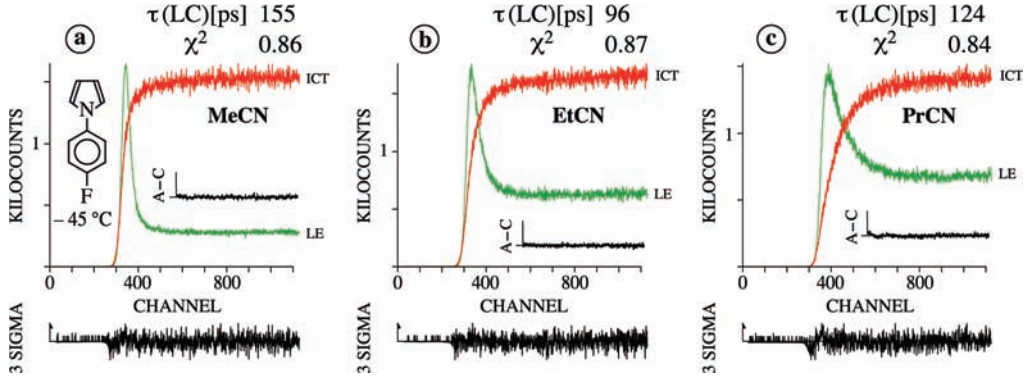

Figure 10. LE and ICT fluorescence decays of PP4F at −45 °C in (a) MeCN, (b) EtCN, and (c) PrCN at 320 nm (LE), 460 nm (ICT, MeCN, EtCN), and 450 nm (ICT, PrCN). The LE/ICT decay times τ(LC) (eq 17) are given in the figure. See the caption of Figure 9.

PP4F in the alkyl cyanides at −45 °C the two excited states LE and ICT are sufficient.

$$\tau(\mathrm{LC}) = 1/(k_d + 1/\tau_0'(\mathrm{ICT})) \qquad (17)$$

Temperature Dependence of the Fluorescence Decay Parameters of PP4F in EtCN. The fluorescence decay times τ_1 and τ_2 (eqs 7 and 8) and the amplitude ratio A (eqs 7−9) of PP4F in EtCN are presented in Figure 11. The lifetime τ_0 of PP4F in isooctane is also depicted. PP4F can be used as the model compound, because ICT does not take place in this solvent (Figure 2a, Table 2). From these data, the temperature dependence of the ICT rate constants k_a and k_d, as well as of the ICT lifetime τ_0'(ICT) can be calculated (Scheme 1).

Thermodynamic Parameters for the ICT Reaction of PP4F in EtCN. The picosecond fluorescence decays of PP4F in EtCN were measured as a function of temperature, from −10 to −90 °C. From the decay times τ_1 and τ_2, the amplitude ratio A, and the decay time τ_0 of the model compound PP4F in isooctane (eqs 7−13, Table 5), the rate constant k_a and k_d> and the ICT lifetime τ_0'(ICT) are calculated (Scheme 1) by employing eqs 14−16. The Arrhenius plots for k_a, k_d, and τ_0'(ICT) are presented in Figure 12. The activation energies E_i and preexponential factors k_i° determined from these plots are collected

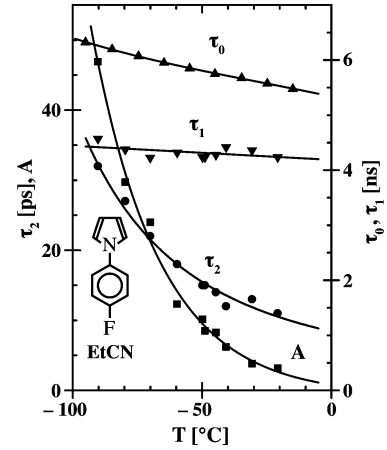

Figure 11. Fluorescence decay parameters for PP4F in EtCN as a function of temperature: decay times τ_1 and τ_2, amplitude ratio A (eqs 7−9). The lifetime τ_0 of the model compound (PP4F in isooctane) is also indicated.

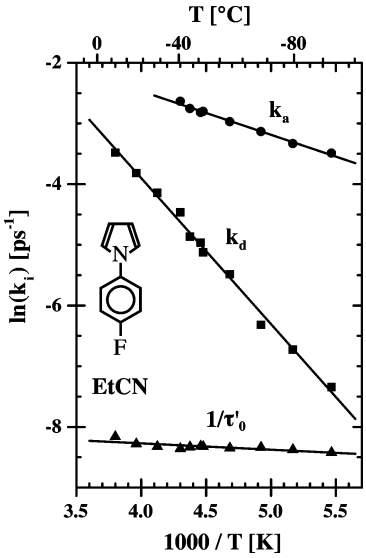

Figure 12. PP4F in EtCN. Arrhenius plots of the forward (k_a) and backward (k_d) ICT rate constants (eqs 14 and 15) vs the reciprocal absolute temperature. The reciprocal ICT lifetime $1/\tau_0'$(ICT) is also shown (eq 16). See Table 6.

in Table 6. The enthalpy difference ΔH is the same as that obtained from the Stevens−Ban plot (Tables 2 and 5, Figure 7b). The lines for k_d and $1/\tau_0'$(ICT) would cross at −104 °C, below the melting point of EtCN. See the section "Stevens−Ban Plots for FPP4F and PP4F. ICT Reaction Enthalpy ΔH(SB)" and Figure 7.

Comparison of Arrhenius Parameters for PP4F, PP, and DMABN. The Arrhenius parameters E_a, E_d, $k_a°$, $k_d°$, ΔH, and ΔS for PP4F in EtCN (Figure 12) are listed together with those for PP and DMABN in Table 6. By introducing a F substituent in PP, $-\Delta H$ increases from 6.7 to 14 kJ/mol. The larger electron affinity[20] of the 4-fluorophenyl subgroup of PP4F as compared with the phenyl group in PP not only leads to an increase of $-\Delta H$, but also results in a decrease of the activation energy E_a from 9.0 to 5.9 kJ/mol. This lowering of the ICT reaction barrier also induces a smaller preexponential factor $k_a°$: 1.5×10^{12} s^{-1} (PP4F) and 4.2×10^{12} s^{-1} (PP). As $k_d°$ similarly correlates with E_d, 300×10^{12} s^{-1} and 20.0 kJ/mol for PP4F versus 109×10^{12} s^{-1} and 15.7 kJ/mol for PP, a correlation between ΔH and ΔS ($= R \ln(k_a°/k_d°)$) is obtained for PP4F relative to PP: −14 and −6.7 kJ/mol versus −44 and −27 J K^{-1} mol^{-1} (Table 6). A similar $\Delta H/\Delta S$ relationship has been observed for intramolecular excimer formation with 1,3-dipyrenylpropanes.[51,52] Such a correlation also appears for PP in the solvent series MeCN, EtCN, and PrCN (Table 6).

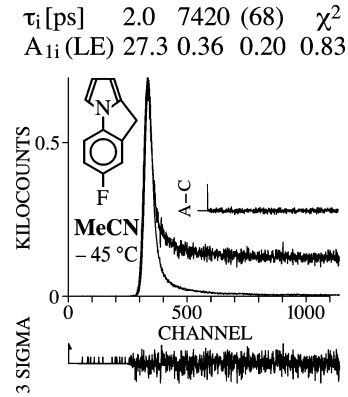

Figure 13. Double-exponential LE fluorescence decay of FPP4F in acetonitrile (MeCN) at −45 °C. The emission wavelength is 320 nm. The decay times τ_2 and τ_1 with the corresponding amplitudes A_{1i}(LE), see eqs 7−11, are given in the figure. The shortest decay time is listed first. The excitation wavelength is 276 nm. The time resolution is 0.496 ps/channel with a time window of 800 effective channels. See the caption of Figure 9.

Picosecond LE Fluorescence Decay of FPP4F in MeCN at −45 °C. The LE fluorescence decay of FPP4F in MeCN at −45 °C (Figure 13) is double-exponential, with decay times $\tau_2 = 2.0$ ps and $\tau_1 = 7.42$ ns and an amplitude ratio $A = 76$ (eqs 7−9). From these data, together with $\tau_0 = 5.64$ ns (FPP4F in isooctane at −45 °C, Table 5), the rate constants k_a and k_d, as well as the ICT lifetime τ_0'(ICT), are again determined (eqs 14−16). It is seen (Table 5) that the k_a of FPP4F (49×10^{10} s^{-1}) is considerably larger than that of PP4F in MeCN at −45 °C (19×10^{10} s^{-1}). A similar finding was reported for the pair FPP/PP (Table 5),[1,2] showing that the planarization in the fluorazenes leads to an increase of the ICT rate constant k_a as compared with that of the corresponding flexible *N*-phenylpyrrole.

With FPP4F in MeCN at 25 °C, a shortest decay time $\tau_2 = 1$ ps is determined (not shown), at the limit of the time resolution (~3 ps)[5] of the picosecond SPC experiments. From the femtosecond excited-state absorption spectra, an ICT reaction time of 1.07 ps is determined; see below (Table 8).

Picosecond LE and ICT Fluorescence Decays of FPP4F in EtCN at −45 and −85 °C. The picosecond LE and ICT fluorescence decays i_f(LE) and i_f(ICT) (eqs 7−9) of FPP4F in EtCN at −45 and −85 °C are shown in Figure 14. With FPP4F at −45 °C, the decay time τ_2 of 2.8 ps (Figure 14a) is shorter than the $\tau_2 = 14.0$ ps of PP4F under these conditions (Figure 9b). Also the LE amplitude ratio A (eq 9)[53] of 40.6 for FPP4F is larger than that of 5.76 for PP4F (Table 5). The analyis of these decay parameters (eqs 14−16) shows that in EtCN at −45 °C the LE → ICT reaction of FPP4F has become considerably

TABLE 6: Activation Energies E_a and E_d, Preexponential Factors $k_a°$ and $k_d°$, Enthalpy Difference ΔH, and Entropy Difference ΔS for the ICT Reaction of PP4F, PP, and DMABN in PrCN, EtCN, and MeCN

	T (°C)	E_a (kJ/mol)	E_d (kJ/mol)	$k_a°$ (10^{12} s^{-1})	$k_d°$ (10^{12} s^{-1})	ΔH^a (kJ/mol)	ΔS^b (J K^{-1} mol^{-1})
				PP4F			
EtCN	−45	5.9	20.0	1.5	300	−14.0	−44
				PP[c]			
PrCN	−45	12.4	17.0	9.2	150	−4.6	−23
EtCN	−45	9.0	15.7	4.2	109	−6.7	−27
MeCN	−45	5.7	15.7	2.1	65	−10.0	−28
				DMABN[d]			
MeCN	−45	5.0	32.0	1.83	186.8	−27.0	−38

[a] $\Delta H = E_a - E_d$. [b] $\Delta S = R \ln(k_a°/k_d°)$. [c] From refs 4 and 33. [d] From ref 5.

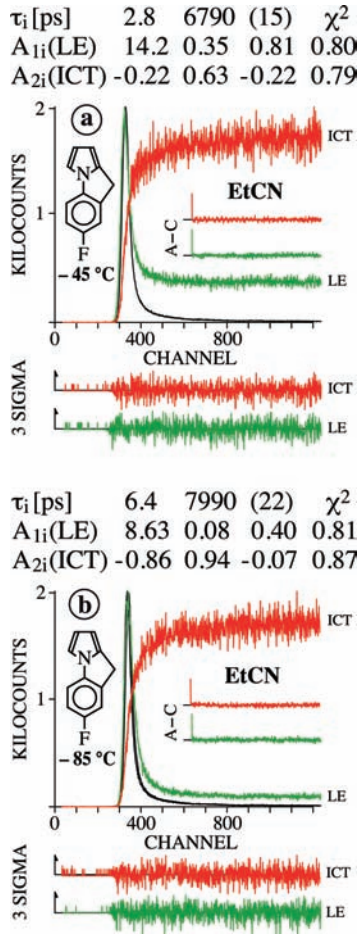

Figure 14. Global analysis for double-exponential LE and ICT fluorescence decays of FPP4F in EtCN at (a) −45 °C and (b) −85 °C. The emission wavelengths are 320 nm (LE) and 460 nm (ICT). The decay times τ_2 and τ_1 with the corresponding amplitudes A_{1i}(LE) and A_{2i}(ICT), see eqs 7−9, are given in the figure. The shortest decay time is listed first. The excitation wavelength is 276 nm. The time in parentheses is attributed to impurities or experimental problems. The time resolution is 0.496 ps/channel with a time window of 800 effective channels. See the caption of Figure 9.

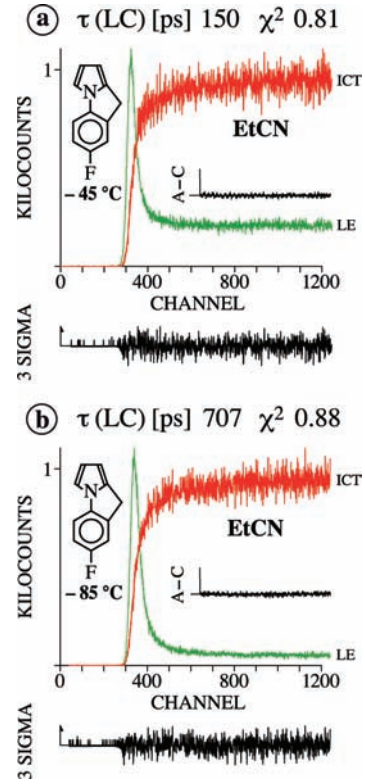

Figure 15. LE and ICT fluorescence decays of FPP4F at (a) −45 °C and (b) −85 °C in EtCN at 315 nm (LE) and at 450 nm (ICT). The LE/ICT decay times τ(LC) (eq 17) are given in the figure. See the caption of Figure 9.

faster than that of PP4F, with k_a(FPP4F) = 35 × 10^{10} s^{-1} and k_a(PP4F) = 6.1 × 10^{10} s^{-1}. At the same time, the ICT back-reaction is somewhat slower for FPP4F than for PP4F: k_d(FPP4F) = 0.86 × 10^{10} s^{-1} and k_d(PP4F) = 1.1 × 10^{10} s^{-1} (Table 5). This last observation could indicate that $-\Delta H$ is in fact larger for FPP4F than for PP4F; see Table 5.

For FPP4F in EtCN at −85 °C (Figure 14b), the decay time τ_2 of 6.4 ps is longer than that of 2.8 ps at −45 °C and the LE, amplitude ratio A (eq 9) has increased from 5.76 to 25.9 between these two temperatures. In terms of rate constants (Table 5), when going from −45 to −85 °C, k_a decreases by a factor of 2, from 6.1 × 10^{10} to 3.2 × 10^{10} s^{-1}, whereas k_d slows more strongly, from 1.1 × 10^{10} to 0.1 × 10^{10} s^{-1}. This behavior is to be expected, as E_d is always larger than E_a for ICT reactions with a negative ΔH: $E_d - E_a = -\Delta H$.[53]

LE/ICT Fluorescence Decay Analysis for FPP4F in EtCN at −45 and −85 °C. The LE/ICT fluorescence decay analysis of FPP4F in EtCN at −45 and −85 °C presented in Figure 15 results in a single decay time τ(LC); see eq 17. This finding supports the applicability of Scheme 1, with only two excited states, LE and ICT, for the description of the ICT reaction with FPP4F. The experimental times τ(LC) show a reasonable agreement with the calculated value $1/(k_d + 1/\tau'_0(\mathrm{ICT}))$ (eq 17), employing the data (Table 5) determined from the global anlysis presented in Figure 14. The agreement is not as good as that obtained for PP4F (Figure 10, Table 5), probably caused by the presence of an additional short decay time in the fluorescence decays (Figure 14).

LE → ICT Reaction Rate Constants for A/D Molecules in EtCN at −45 °C (Table 5). For PP and PP4F in EtCN at −45 °C, the rate constant k_a increases with increasing electron acceptor strength of the moieties phenyl and fluorophenyl: 3.9 × 10^{10} and 6.1 × 10^{10} s^{-1}, respectively. A similar development is obtained for FPP and FPP4F: 8.2 × 10^{10} and 34.8 × 10^{10} s^{-1}. With FPP4C and PP4C, having a strongly electronegative benzonitrile group as discussed in the Introduction, the ICT reaction is much faster than with FFP4F/PP4F.[2,54]

It is obvious that the molecular rigidization introduced by the $-CH_2-$ linkage in the fluorazenes leads to a substantial increase of k_a as compared with the corresponding *N*-phenylpyrroles: 8.2 × 10^{10} and 3.9 × 10^{10} s^{-1} for FPP/PP, 35 × 10^{10} and 6.1 × 10^{10} s^{-1} for FPP4F/PP4F (Table 5). Also the ICT reaction enthalpies $-\Delta H$ of the fluorazenes are larger than those of the *N*-phenylpyrroles in MeCN: −15.1 and −10.0 kJ/mol (FPP/PP) and −19.2 and −14.9 kJ/mol (FPP4F/PP4F).

Rate Constants k_a in MeCN at −45 °C. In MeCN at −45 °C, the following rate constants k_a (10^{10} s^{-1}) are obtained: 49 (FPP4F), 19 (PP4F), 9.9 (PP), and 13.1 (DMABN). For the *N*-phenylpyrroles and their derivatives in MeCN, the reaction enthalpy $-\Delta H$ (kJ/mol) shows a correlation with k_a: 19.2 (FPP4F), 14.9 (PP4F), and 10.0 (PP). DMABN (27.0 kJ/mol) does not fit into this correlation; see Table 5. A similar correlation is found between ΔG and k_a.

Transient Absorption Spectra of FPP4F in *n*-Hexane. The transient absorption spectra of FPP4F in *n*-hexane at 290 nm excitation (Figures 16a and S1a in the Supporting Information)

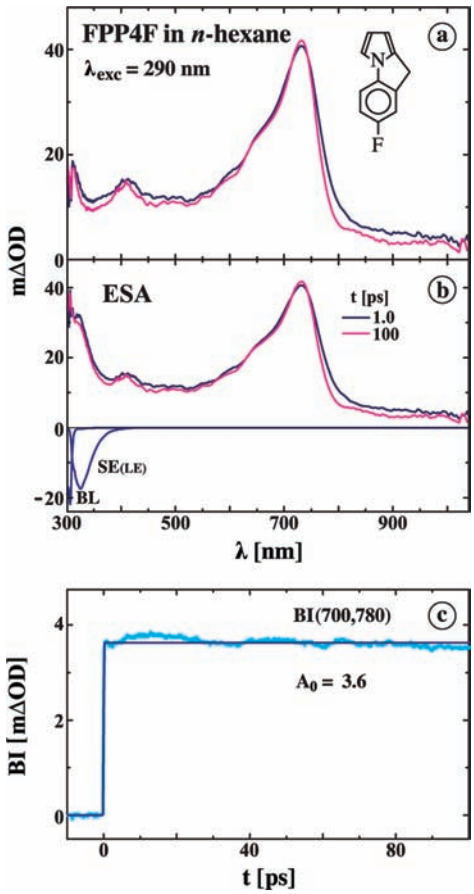

Figure 16. FPP4F in *n*-hexane at 290 nm excitation. (a) Transient absorption spectra and (b) ESA spectra after subtraction of the bleach (BL) and SE, at pump−probe delay times of 1.0 and 100 ps. The SE spectrum (LE; cf. Figure 2e) and the BL are also depicted. The spectral range extends from 300 to 1040 nm. (c) The band integral BI(700,780), between 700 and 780 in the ESA spectrum, does not show any time development. The offset A_0 (eq 18) is also indicated. mΔOD is the optical density/1000.

consist of a main band with a maximum at 730 nm (Table 7). After subtraction of the stimulated emission (SE), the ESA spectra are obtained (Figure 16b). As only an LE emission is observed in the fluorescence spectrum of FPP4F in *n*-hexane (Figure 2e), the ESA band is attributed to the LE state. The band integral BI(700,780), between 700 and 780 nm in the ESA spectrum, does not show any time development (Figure 16c). With an excitation wavelength of 266 nm, practically the same ESA spectrum results (Figure S2, Supporting Information).

$$\mathrm{BI} = A_2 \exp(-t/\tau_2) + A_1 \exp(-t/\tau_1) + A_0 \qquad (18)$$

Transient Absorption Spectra of PP4F in *n*-Hexane. The transient absorption spectra of PP4F in *n*-hexane at 290 nm excitation, for pump−probe delay times of 1.0 and 100 ps and between 0.4 and 120 ps, are shown in Figures 17a and S3a (Supporting Information). The ESA spectra, obtained by subtracting the stimulated emission (Figures 17b and S3b), again consist of a main band, with a maximum at 740 nm (Table 7). The spectra show a close similarity with those of FPP4F (Figure 16). As an ICT reaction does not take place for PP4F in *n*-hexane (Figure 2a), the ESA spectra are therefore likewise attributed to the LE state. The band integral BI(700,780) of PP4F does not show a decay. At 266 nm excitation, a similar LE ESA spectrum is measured for PP4F in *n*-hexane (Figure S4,

TABLE 7: ESA Maxima for FPP4F, PP4F, and PP4M in *n*-Hexane and MeCN at 290 and 266 nm Excitation[a]

	ESA maxima (nm) (excitation wavelength λ_{exc})	
	n-hexane	MeCN
FPP4F	320, 410, **730** (290 nm),[c,d] 410, **733** (266 nm)[d]	295,[b] 325, (405), **735** (290 nm),[d,e] **730** (266 nm)[d]
PP4F	315, 415, 495, **740** (290 nm),[d,f] 415, 495, **744** (266 nm)[d]	320, 405[b], **740** (290 nm)[d,e] 400[b], **747** (266 nm)[d]
PP4M		400, 496, 525, **770** (290 nm)[d]
FPP4C[d,g]	**444**, 699 (290 nm)	**377**, 499, 730[h] (290 nm)
PP4C[d,g]	**378**, **444**, **729** (290 nm)	below 340, 453, 750[h] (290 nm)
DMABN (LE) [f,i]	**300**−**320**, 445, **745** (290 nm)	320, **355**, 440, **710** (290 nm)
DMABN (ICT) [f,i]		**315**, 425 (290 nm)
NTC6 (LE)[d,j]	**470**[j], **800**[k] (290 nm)	
NTC6 (ICT)[d,j]		below 340[l], 435[l] (290 nm)

[a] See Figures 16−20 and S1−S8 (Supporting Information). Data for FPP4C, PP4C, NTC6, and DMABN are also included. The main maxima are in bold. [b] ICT ESA band. All other maxima are for LE bands. [c] Spectral range 300−1040 nm. [d] Spectral range 340−1040 nm. [e] Spectral range 285−1040 nm. [f] Spectral range 285−1070 nm. [g] Data from ref 2. [h] LE absorption at a delay time of 70 fs (ref 2). [i] From ref 5. [j] From ref 24. [k] At a 200 fs pump−probe delay time. [l] At a 5 ps delay time.

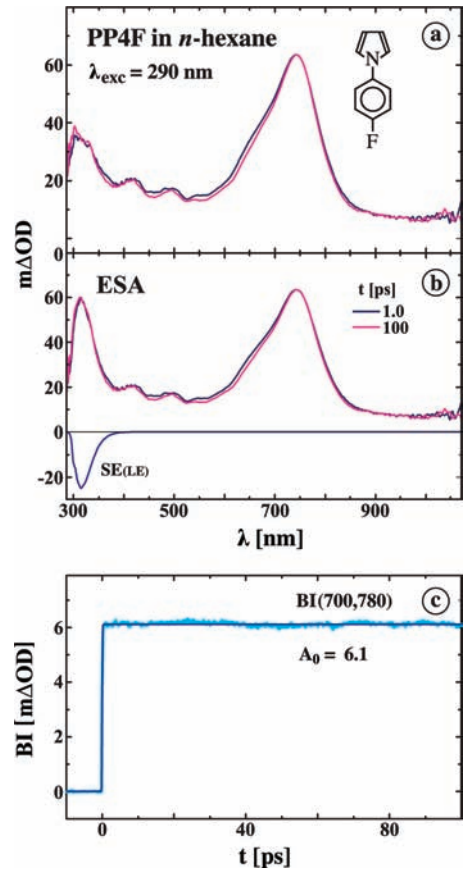

Figure 17. PP4F in *n*-hexane at 290 nm excitation. (a) Transient absorption spectra and (b) ESA spectra, attributed to LE, after subtraction of the SE, at pump−probe delay times of 1.0 and 100 ps. The spectral range extends from 285 to 1070 nm. (c) The band integral BI(700,780) does not show a time development. See the caption of Figure 16.

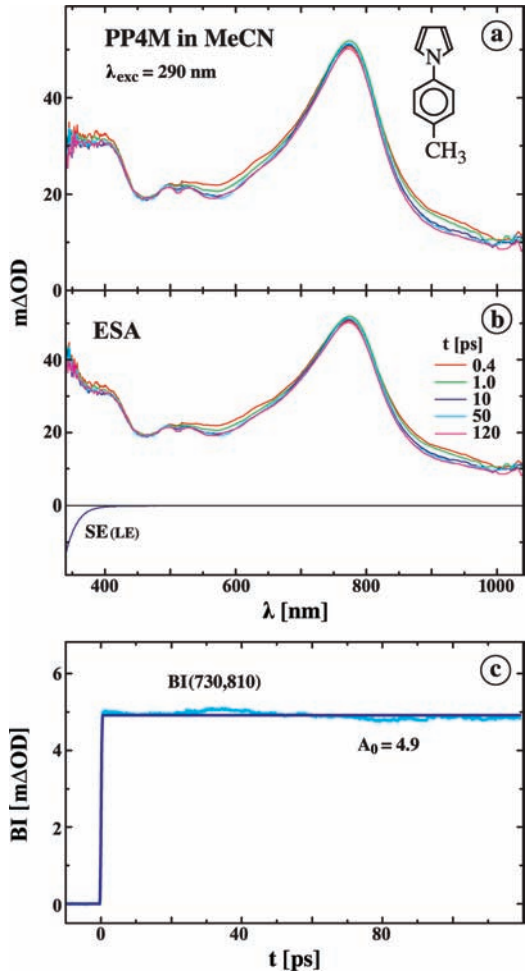

Figure 18. PP4M in MeCN at 290 nm excitation. (a) Transient absorption spectra and (b) ESA spectra after subtraction of the SE, at pump−probe delay times between 0.4 and 120 ps. The SE spectrum (LE; see ref 3) is also depicted. The spectral range extends from 340 to 1040 nm. (c) The band integral BI(730,810) does not decay with time. See the caption of Figure 16.

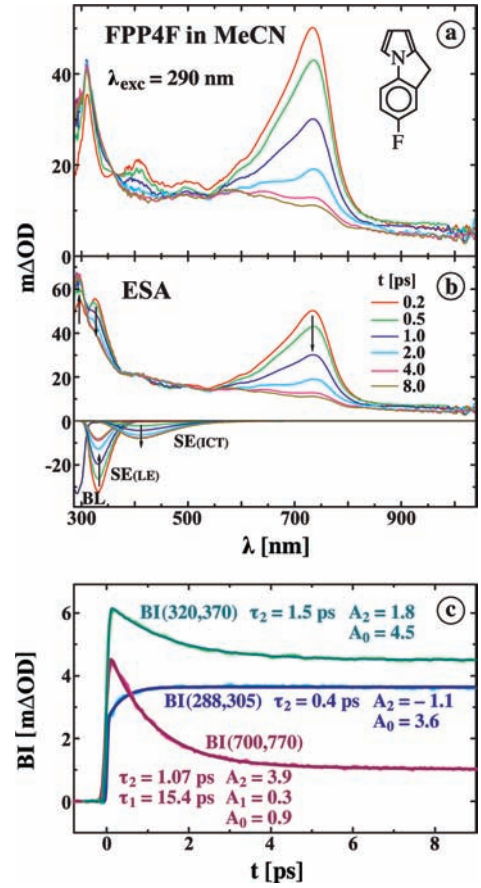

Figure 19. FPP4F in MeCN at 290 nm excitation. (a) Transient absorption spectra and (b) ESA spectra after correction for the BL, SE(LE), and SE(ICT), with pump−probe delay times between 0.2 and 8.0 ps. The SE(LE) and SE(ICT) spectra and their time development are also shown. The downward arrow (735 nm) represents the decay of the LE state. The spectral range extends from 285 to 1040 nm. (c) Analysis (eq 18) of the band integrals BI(700,770), BI(288,305), and BI(320,370). A global analysis of the three BIs results in a time τ_2 of 1.2 ps. Note the growing-in of BI(288,305) in the spectral range of the ICT absorption. See the caption of Figure 16.

Supporting Information). In this case, BI(700,780) grows-in with a time of 9 ps, probably caused by vibrational cooling, as observed for the ICT reaction of FPP4C/PP4C, DMABN, and NTC6.[2,5,24]

LE ESA Spectrum of PP4M. The transient absorption and ESA spectra of PP4M in MeCN at pump−probe delay times between 0.4 and 120 ps are shown in Figure 18. From the fact that PP4M does not undergo an ICT reaction, irrespective of the solvent polarity,[3,4] it follows that the ESA spectra in Figure 18b, with a main maximum at 770 nm, are those of the LE state of PP4M in MeCN. Their similarity with the ESA spectra of FPP4F and PP4F in *n*-hexane (Figures 16b and 17b) fully supports the identification of these spectra as those of an LE state.

Transient Absorption Spectra of FPP4F in MeCN. The transient absorption spectra of FPP4F in MeCN at an excitation wavelength of 290 nm are shown in Figure 19a. After correction for bleaching and stimulated emission, the ESA spectra are obtained for pump−probe delay times between 0.2 and 8.0 ps (Figure 19b). The ESA absorption peaks at 735 and 325 nm are attributed to the LE state, on the basis of the similarity with the ESA spectra of FPP4F in *n*-hexane (Figure 16b). BI(700,770) decays with a time τ_2 of 1.07 ps. This time τ_2 is the LE → ICT reaction time of FPP4F in MeCN (Table 8). The ESA peak at 295 nm is attributed to the absorption of the ICT state. A growing-in of this ICT absorption band is found for BI(288,305), with a rise time of 1.2 ps obtained from a global analysis (not shown) of the three BIs in Figure 19c; see Table 8. From the transient absorption and ESA spectra of FPP4F in MeCN at 290 and 266 nm excitation (Figures S5a and S6b, Supporting Information), with pump−probe delay times between 0.2 and 120 ps, similar decay times τ_2 of 1.07 ps (290 nm) and 0.91 ps (266 nm) are determined from BI(700,770). The longer decay times τ_1 of 15.4 ps (Figure S5c, Supporting Information) and

TABLE 8: Decay Time and LE → ICT Reaction Rate Constant Derived from Femtosecond ESA Spectra of FPP4F, PP4F, FPP4C, PP4C, and DMABN in MeCN at 22 °C

	τ_2[a] (ps)	k_a[b,c] (10^{10} s^{-1})
FPP4F	1.2[d]	94
PP4F	3.3	30
FPP4C[e]	0.087[f]	1150
PP4C[e]	0.067[f]	1500
DMABN[g]	4.07	24.6

[a] See eq 7. [b] See Scheme 1. [c] Calculated by $k_a = 1/\tau_2$. This value is an upper limit; see ref 53. [d] From global analysis; see the caption of Figure 19. [e] From ref 2. [f] Shortest decay time in the femtosecond excited-state absorption spectrum (ref 2). [g] From ref 5.

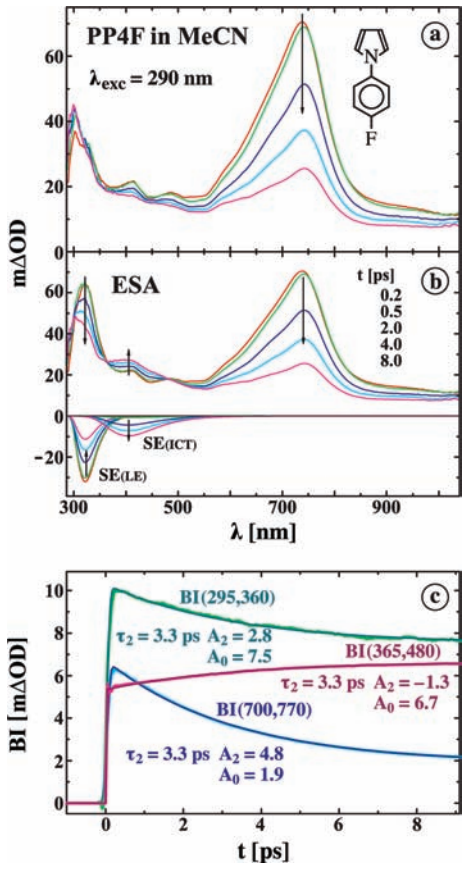

Figure 20. PP4F in MeCN at 290 nm excitation. (a) Transient absorption spectra and (b) ESA spectra after subtraction of SE(LE) and SE(ICT), at pump−probe delay times between 0.2 and 8.0 ps. The time development of the SE(ICT) and SE(LE) emission spectra is also shown. In (b), the downward arrows (740 and 320 nm) indicate the decay of the LE absorption, whereas the upward arrow (405 nm) represents the growing-in of the ICT absorption. The spectral range extends from 285 to 1040 nm. (c) Decay curves of the band integrals BI(700,770), BI(365,480), and BI(295,360). A global analysis of the three BIs results in a time τ_2 of 3.3 ps. Note the growing-in of BI(365,480) in the spectral range of the ICT absorption. See the caption of Figure 16.

9.1 ps (Figure S6c, Supporting Information) are again due to vibrational cooling.[2,5,24]

Transient Absorption Spectra of PP4F in MeCN. The transient absorption spectra of PP4F in MeCN at an excitation wavelength of 290 nm are presented in Figures 20a and S7a (Supporting Information). After correction of the contribution from LE and ICT SE spectra, the ESA spectra are obtained (Figure 20b). The absorption peaks at 740 and 320 nm are part of the LE ESA spectrum. Both bands show a decay with a time τ_2 of 3.3 ps (Figure 20c). This time corresponds to the LE → ICT reaction time (Table 8). For BI(365,480) covering part of the ICT ESA spectrum, a growing-in is observed. At 266 nm excitation (Figure S8c, Supporting Information) $\tau_2 = 2.94$ ps.

LE and ICT ESA Maxima (Table 7). The main maxima in the LE ESA spectra of FPP4F and PP4F in *n*-hexane are at 730 and 740 nm, respectively. A similar main ESA band is observed in MeCN at 735 nm (FPP4F) and at 740 nm (PP4F). As their intensity decays with time (Figures 19 and 20), these bands are likewise attributed to the LE state. A second weaker LE absorption maximum occurs at around 320 nm (Table 7). In the present investigations, covering the spectral range 285−1040 nm, only relatively weak ICT ESA bands are detected. With FPP4F in MeCN a growing-in is detected at 295 nm. Similarly, a rise is found for PP4F in MeCN at around 405 nm (Table 7).

The LE ESA spectra of FPP4F and PP4F, having maxima around 740 nm, show a similarity to those of DMABN, FPP4C/PP4C, and NTC6. Also in MeCN the ICT ESA spectra of FPP4F and PP4F in MeCN have maxima comparable with those of DMABN, FPP4C/PP4C, and NTC6 (Table 7). These similarities support our interpretation (PICT model) that the ICT state of these A/D molecules has a planar structure.[1−6,24,33,40]

Conclusions

The pyrrole subgroup in crystalline PP4F is twisted over an angle θ of 25° relative to the fluorobenzene moiety, whereas FPP4F is as expected practically planar in the crystal, with $\theta = 2°$. Structural differences reside mainly in the phenyl−pyrrole bond length (140.7 pm for FPP4F and 141.8 pm for PP4F), influencing the electronic coupling between the two groups, as well as in the absence of symmetry along the long axis of FPP4F due to the $-CH_2-$ linkage. An ICT reaction with the appearance of LE + ICT dual fluorescence takes place with FPP4F and PP4F in solvents of medium polarity, whereas only LE emission is observed in alkane solvents such as *n*-hexane. The LE → ICT reaction is more pronounced for FPP4F than with PP4F, caused by a smaller energy gap $\Delta E(S_1,S_2)$, in accordance with the PICT model. The occurrence of an ICT reaction is confirmed by the dipole moments determined from the two fluorescence bands, with μ_e(ICT) = 12 D (FPP4F) and 10 D (PP4F), clearly larger than μ_e(LE) of ∼4 D for FPP4F and PP4F.

In the fluorescence spectra of FPP4F and PPF4 in MeCN, EtCN, and PrCN measured as function of temperature, isoemissive points appear, confirming the two-state (LE and ICT) reaction mechanism. From the Stevens−Ban plots of ln(Φ′(ICT)/Φ(LE)) vs 1000/*T* for FPP4F and PP4F, the ICT reaction enthalpy ΔH(SB) (= $E_a - E_d$) is obtained. $-\Delta H$(SB) decreases when the solvent polarity becomes smaller, from 19.2 kJ/mol in MeCN to 16.5 kJ/mol in PrCN for FPP4F and from 14.9 kJ/mol in MeCN to 12.6 kJ/mol in PrCN for PP4F. Larger $-\Delta H$(SB) values are determined for FPP4F than with PP4F, establishing that the rigidization by the methylene linkage leads to more efficient ICT.

From picosecond fluorescence decays of PP4F in MeCN, EtCN, and PrCN at −45 °C it is found that the forward ICT rate constant k_a in this solvent series decreases from 19×10^{10} via 6.1×10^{10} to 2.1×10^{10} s^{-1}, as the sovent polarity ε becomes smaller: 50.2 (MeCN), 39.0 (EtCN), and 35.1 (PrCN). The deconvolution of the ICT decays with their corresponding LE decays as the virtual excitation pulse results in single-exponential decay times τ(LC) equal to $1/(k_d + 1/\tau_0'(\text{ICT}))$, supporting the correctness of the decay analysis within the two-state (LE + ICT) reaction scheme. The LE decays of PP4F in EtCN between −10 and −90 °C give rate constants k_a and k_d, from which the activation energies E_a (5.9 kJ/mol) and E_d (20.0 kJ/mol) and hence the ICT reaction enthalpy $\Delta H = -14.0$ kJ/mol (the same as ΔH(SB)) are determined. With FPP4F, shorter decay times τ_2 are measured than those of PP4F, pointing to a faster ICT process at the experimental limit of the fluorescence decay experiments.

The ESA spectra of FPP4F and PP4F predominantly consist of LE absorption bands. These LE spectra are identified via the ESA spectrum of PP4M, not undergoing an ICT reaction, irrespective of the solvent polarity. The LE spectra of FPP4F

and PP4F in *n*-hexane do not show any time development (except vibrational cooling), which shows that an ICT reaction does not take place in this solvent. The rapid decay observed for the ESA spectra of FPP4F and PP4F in MeCN is caused by ICT, with reaction times of 1.1 ps (FPP4F) and 3.3 ps (PP4F) at 22 °C. The shape of the LE spectrum of FPP4F and PP4F in *n*-hexane and that of PP4M in MeCN support our previous identification of the LE and ICT ESA spectra of FPP4C and PP4C, compounds for which the establishment of an ultrafast kinetic equilibrium in *n*-hexane complicates the analysis. The finding that FPP4F and PP4F have a planar ICT state, on the basis of the similarity of their ICT spectra, is further support for our previous conclusion (PICT model) that the ICT states of FPP4C/PP4C, FPP/PP, and NTC6/DMABN have a planar molecular structure. These results again make clear that a perpendicular twist of the donor and acceptor subgroups in a D/A molecule is not a requirement for fast and efficient ICT.

Acknowledgment. Many thanks are due to Prof. N. P. Ernsting (Humboldt University Berlin) for the use of the femtosecond absorption equipment in the investigations reported here. We are grateful to Mr. W. Bosch for the synthesis of FPP4F. We also thank Mr. J. Bienert for carrying out HPLC purifications and Mr. H. Lesche for technical support. A.D. gratefully acknowledges the support of the Hungarian Science Foundation (OTKA ID No. 76278).

Supporting Information Available: Excited-state absorption spectra of FPP4F and PP4F in *n*-hexane and MeCN. This material is available free of charge via the Internet at http://pubs.acs.org.

References and Notes

(1) Yoshihara, T.; Druzhinin, S. I.; Zachariasse, K. A. *J. Am. Chem. Soc.* **2004**, *126*, 8535.

(2) Druzhinin, S. I.; Kovalenko, S. A.; Senyushkina, T. A.; Demeter, A.; Machinek, R.; Noltemeyer, M.; Zachariasse, K. A. *J. Phys. Chem. A* **2008**, *112*, 8238; Erratum. *J. Phys. Chem. A* **2009**, *113*, 520.

(3) Yoshihara, T.; Galievsky, V. A.; Druzhinin, S. I.; Saha, S.; Zachariasse, K. A. *Photochem. Photobiol. Sci.* **2003**, *2*, 342.

(4) Yoshihara, T.; Druzhinin, S. I.; Demeter, A.; Kocher, N.; Stalke, D.; Zachariasse, K. A. *J. Phys. Chem. A* **2005**, *109*, 1497.

(5) Druzhinin, S. I.; Ernsting, N. P.; Kovalenko, S. A.; Lustres, L. P.; Senyushkina, T. A.; Zachariasse, K. A. *J. Phys. Chem. A* **2006**, *110*, 2955.

(6) Galievsky, V. A.; Druzhinin, S. I.; Demeter, A.; Jiang, Y.-B.; Kovalenko, S. A.; Lustres, L. P.; Venugopal, K.; Ernsting, N. P.; Allonas, X.; Noltemeyer, M.; Machinek, R.; Zachariasse, K. A. *ChemPhysChem* **2005**, *6*, 2307.

(7) Mortensen, J.; Heinze, J. *Angew. Chem.* **1984**, *96*, 64.

(8) In an electron D/A molecule with substantial electronic coupling between the D and A subgroups, such as in DMABN, the energy of the ICT state (A^-D^+) expressed in terms of the difference in the redox potentials, $E(\mathrm{ICT}) \cong f(E(\mathrm{D/D^+}) - E(\mathrm{A^-/A})) + C$, does decrease more slowly ($f < 1$) than the reduction potential $E(\mathrm{A^-/A})$ or electron affinity of the acceptor moiety (refs 9−12). In fact, primarily the energy difference between the two lowest singlet excited states $\Delta E(S_1,S_2)$ is the determining factor for the occurrence of an ICT reaction. A recent example of this situation is found with tricyanoanilines such as 2,4,6-tricyano-*N*,*N*-dimethylaniline (TCDMA); see ref 12.

(9) von der Haar, Th.; Hebecker, A.; Il'ichev, Yu. V.; Jiang, Y.-B.; Kühnle, W.; Zachariasse, K. A. *Recl. Trav. Chim. Pays-Bas* **1995**, *114*, 430.

(10) Il'ichev, Yu. V.; Kühnle, W.; Zachariasse, K. A. *J. Phys. Chem. A* **1998**, *102*, 5670.

(11) Galievsky, V. A.; Zachariasse, K. A. *Acta Phys. Pol., A* **2007**, *112*, S-39.

(12) Zachariasse, K. A.; Druzhinin, S. I.; Galievsky, V. A.; Kovalenko, S.; Senyushkina, T. A.; Mayer, P.; Noltemeyer, M.; Boggio-Pasqua, M.; Robb, M. A. *J. Phys. Chem. A* **2009**, *113*, 2693.

(13) Berlman, I. B. *Handbook of Fluorescence Spectra of Aromatic Molecules*; Academic Press: New York, 1971.

(14) Cogan, S.; Zilberg, S.; Haas, Y. *J. Am. Chem. Soc.* **2006**, *128*, 3335.

(15) Grabowski, Z. R.; Rotkiewicz, K.; Rettig, W. *Chem. Rev.* **2003**, *103*, 3899.

(16) Lippert, E.; Lüder, W.; Boos, H. In *Advances in Molecular Spectroscopy*, European Conference on Molecular Spectroscopy, Bologna, Italy, 1959; Mangini, A., Ed.; Pergamon Press: Oxford, U.K., 1962; p 443.

(17) Lippert, E.; Lüder, W.; Moll, F.; Nägele, W.; Boos, H.; Prigge, H.; Seibold-Blankenstein, I. *Angew. Chem.* **1961**, *73*, 695.

(18) Grabowski, Z. R.; Rotkiewicz, K.; Rubaszewska, W.; Kirkor-Kaminska, E. *Acta Phys. Pol.* **1978**, *54A*, 767.

(19) Rettig, W.; Wermuth, G.; Lippert, E. *Ber. Bunsenges. Phys. Chem.* **1979**, *83*, 692.

(20) The difference in electron acceptor strength of a fluoro and cyano substituent can be deduced from the reduction potentials $E(\mathrm{A^-/A})$ of fluorobenzene (−2.75 V vs SCE, ref 21) and benzonitrile (−2.36 V vs SCE, ref 6). By comparing the reduction potentials (ref 21) of hexafluorobenzene (−2.11 V vs SCE), pentafluorobenzene (−2.35 V vs SCE), and benzonitrile (−2.30 V vs SCE), it is seen that between five and six F atoms are needed to achieve an increase in the acceptor strength of the phenyl moiety similar to that brought about by a single CN group. Note that, as mentioned above, $E(\mathrm{A^-/A}) = -2.36$ V vs SCE has been reported in ref 6.

(21) Loutfy, R. O.; Loutfy, R. O. *Can. J. Chem.* **1976**, *54*, 1454.

(22) Elming, N.; Clauson-Kaas, N. *Acta Chem. Scand.* **1952**, *6*, 867.

(23) Bailey, A. S.; Scott, P. W.; Vandrevala, M. H. *J. Chem. Soc., Perkin Trans. 1* **1980**, 97.

(24) Druzhinin, S. I.; Kovalenko, S. A.; Senyushkina, T.; Zachariasse, K. A. *J. Phys. Chem. A* **2007**, *111*, 12878.

(25) Demas, J. N.; Crosby, G. A. *J. Phys. Chem.* **1971**, *75*, 991.

(26) Druzhinin, S. I.; Galievsky, V. A.; Zachariasse, K. A. *J. Phys. Chem. A* **2005**, *109*, 11213.

(27) Kocher, N.; Leusser, D.; Meindl, K.; Henn, J.; Zachariasse, K. A.; Sheldrick, G. M.; Koritsanszky, T.; Stalke, D. *J. Phys. Chem. A*, in press.

(28) von Bülow, R. Diplomarbeit (Master Thesis), University of Göttingen, 1996.

(29) Schweke, D.; Abramov, S.; Haas, Y. *Chem. Phys.* **2007**, *335*, 87.

(30) Cornelissen-Gude, C.; Rettig, W. *J. Phys. Chem. A* **1998**, *102*, 7754.

(31) Rückert, I.; Hebecker, A.; Parusel, A. B. J.; Zachariasse, K. A. *Z. Phys. Chem.* **2000**, *214*, 1597.

(32) (a) Rückert, I.; Demeter, A.; Morawski, O.; Kühnle, W.; Tauer, E.; Zachariasse, K. A. *J. Phys. Chem. A* **1999**, *103*, 1958. (b) Zachariasse, K. A.; Grobys, M.; von der Haar, Th.; Hebecker, A.; Il'ichev, Yu. V.; Jiang, Y.-B.; Morawski, O.; Kühnle, W. *J. Photochem. Photobiol., A* **1996**, *102*, 59; Erratum. *J. Photochem. Photobiol., A* **1998**, *115*, 259.

(33) Druzhinin, S. I.; Galievsky, V. A.; Yoshihara, T.; Zachariasse, K. A. *J. Phys. Chem. A* **2006**, *110*, 12760.

(34) In the subtraction procedure to separate a weak ICT emission from the main LE fluorescence band, the problem arises that the fluorescence spectrum adopted for LE is not exactly that of the LE emission, but rather that of a model compound, such as PP4M employed here, which is at best similar but certainly not identical to the real LE fluorescence band. For this reason, $\Phi'(\mathrm{ICT})/\Phi(\mathrm{LE})$ ratios of 0.02 such as reported by us (ref 4) for PP in THF at 25 °C are at the limit of the possible experimental accuracy, although the value of 0.02 was obtained by analyzing a series of measurements as a function of temperature in THF, with $\Phi'(\mathrm{ICT})/\Phi(\mathrm{LE}) = 0.05$ at −104 °C (ref 4).

(35) Il'ichev, Yu, V.; Kühnle, W.; Zachariasse, K. A. *Chem. Phys.* **1996**, *211*, 441.

(36) Suppan, P.; Ghoneim, N. *Solvatochromism*; The Royal Society of Chemistry: Cambridge, U.K., 1997.

(37) Liptay, W. In *Excited States*; Lim, E. C., Ed.; Academic Press: New York, 1974, Vol. 1, p 129.

(38) Baumann, W.; Bischof, H.; Brittinger, J.-C.; Rettig, W.; Rotkiewicz, K. *J. Photochem. Photobiol., A* **1992**, *64*, 49.

(39) Demeter, A.; Druzhinin, S.; George, M.; Haselbach, E.; Roulin, J.-L.; Zachariasse, K. A. *Chem. Phys. Lett.* **2000**, *323*, 351.

(40) Zachariasse, K. A.; Druzhinin, S. I.; Bosch, W.; Machinek, R. *J. Am. Chem. Soc.* **2004**, *126*, 1705.

(41) Hedestrand, G. *Z. Phys. Chem. B* **1929**, *2*, 428.

(42) At −45 °C, the dielectric constants are the following: 50.2 (MeCN), 39.0 (EtCN), 35.1 (PrCN) (see ref 4).

(43) Landolt-Börnstein. In *Numerical Data and Functional Relationships in Science and Technology, New Series*; Madelung, O., Ed.; Springer: Berlin, 1991; Vol. 6, Group IV.

(44) Leinhos, U.; Kühnle, W.; Zachariasse, K. A. *J. Phys. Chem.* **1991**, *95*, 2013.

(45) Stevens, B.; Ban, M. I. *Trans. Faraday Soc.* **1964**, *60*, 1515.

(46) Birks, J. B. *Photophysics of Aromatic Molecules*; Wiley: London, 1970.

(47) Gómez, I.; Reguero, M.; Boggio-Pasqua, M.; Robb, M. A. *J. Am. Chem. Soc.* **2005**, *127*, 7119.

(48) Gómez, I.; Mercier, Y.; Reguero, M. *J. Phys. Chem. A* **2006**, *110*, 11455.

(49) Conte, J. C.; Martinho, J. M. G. *Chem. Phys. Lett.* **1987**, *134*, 350.

(50) Zachariasse, K. A.; Yoshihara, T.; Druzhinin, S. I. *J. Phys. Chem. A* **2002**, *106*, 6325; Erratum. *J. Phys. Chem. A* **2002**, *106*, 8978.

(51) Duveneck, G.; Zachariasse, K. A. *J. Am. Chem. Soc.* **1987**, *109*, 3790.

(52) Williams, A. *Free Energy Relationships in Organic and Bio-organic Chemistry*; The Royal Society of Chemistry: Cambridge, U.K., 2003.

(53) For the LE amplitude ratio the following expression holds: $A = (X - 1/\tau_1)/(1/\tau_2 - X)$ (see eq 11). With $X = k_a + 1/\tau_0$ (eq 12), $A = (k_a + 1/\tau_0 - 1/\tau_1)/(1/\tau_2 - k_a - 1/\tau_0)$. By employing the equation $1/\tau_1 + 1/\tau_2 = k_a + 1/\tau_0 + k_d + 1/\tau_0'(\mathrm{ICT})$ (eqs 10, 12, and 13), it follows that, under the conditions k_a, $k_d \gg 1/\tau_0 + 1/\tau_0'(\mathrm{ICT})$, and $1/\tau_2 \gg 1/\tau_1$ (see Figures 9, 13, and 14), one obtains $A \cong k_a/k_d$. Under the same conditions one finds $1/\tau_2 = k_a + k_d$. In general, the reciprocal decay time τ_2 equals the sum of the forward and backward ICT reaction rate constants (Scheme 1). Obviously, therefore, only in cases where $k_a \gg k_d$, one can conclude that $1/\tau_2 \cong k_a$. This will be the case for A/D molecules with sufficiently large reaction enthalpies $-\Delta H$, such as for DMABN in MeCN (ref 5) and also for FPP4C and PP4C in this solvent (ref 2). With DMABN in MeCN, $\Delta H = -27$ kJ/mol. For FPP4C and PP4C, $\Delta H = -11$ and -7 kJ/mol, respectively, already in *n*-hexane, whereas in MeCN $-\Delta H$ is much larger for these molecules, as evidence for the back-reaction could not be detected, which means that $k_a \gg k_d$ (ref 2). The ΔH in MeCN for the systems investigated here is -19.2 kJ/mol (FPP4F) and -14.9 kJ/mol (PP4F) smaller than for DMABN. This makes the ratio k_a/k_d smaller, and k_d can therefore no longer be neglected with respect to k_a. As a result, the reciprocal of the ESA decay times τ_2 in Table 8 only is an upper limit for the LE → ICT reaction rate constant k_a; see Table 5.

(54) With FPP4C and PP4C in *n*-hexane at 22 °C (ref 2), the ICT reaction time is 0.65 and 0.48 ps, respectively, leading to rate constants k_a of 1.5×10^{12} and 2.1×10^{12} s^{-1}. In MeCN at this temperature, much shorter reaction times and larger k_a values are obtained: 87 fs (11×10^{12} s^{-1}) for FPP4C and 67 fs (15×10^{12} s^{-1}) for PP4C. Although the ICT reaction for FPP4C/PP4C will become somewhat slower in EtCN at −45 °C, it will nevertheless remain much faster than that for the pairs FPP/PP and FPP4F/PP4F. In support of this conclusion, only ICT fluorescence is observed with FPP4C and PP4C in EtCN at −45 °C (ref 2).

JP903613C